Estimating Axial Force Demand in Columns of Shear-Type Structure Subjected to Earthquake-Base Excitation

Lisa Shrestha, Aff.M.ASCE[1]; and Michel Bruneau, F.ASCE[2]

Abstract: A procedure for estimating the number of simultaneously yielding stories N_{SYS} in a shear-type building subjected to earthquake-base excitation (previously proposed and validated) is used here for estimating axial force demand in the columns of such structures. Axial force demand of a column is obtained by summing the vertical force transferred by the N_{SYS} simultaneously yielding stories with a square root of sum of squares (SRSS) combination of the forces that could be transferred by the remaining stories above that column, considering their full yield capacity. Axial force in the columns due to the simultaneous story yielding caused by the incident velocity wave and overlapping of the incident and reflected velocity waves occurring at the top and bottom of the building are considered. Three categories of earthquakes, namely earthquake excitations having (1) a single dominant pulse, (2) multiple distinct pulses, and (3) no distinct pulses in their velocity record, are considered. Also presented are results from a parametric study conducted by varying column stiffness and strain hardening of the brace members. The procedures for estimating the number of simultaneously yielding stories and axial force demand proposed here were found to provide good estimates of the values developed during actual earthquake excitations, especially for the first two categories of earthquakes, with the estimated values generally being on the conservative side. The procedures were also found to work well for the range of column stiffness and strain hardening ratios considered in the parametric study. **DOI: 10.1061/(ASCE)ST.1943-541X.0002086.**

Author keywords: Simultaneous story yielding; Axial force demand; Column design; Wave propagation; Seismic design; Multistory buildings; Shear buildings; Buckling-restrained brace frame.

Introduction

Consideration of full yield capacity of the ductile members at all floors of a building, with an assumption that they undergo yielding simultaneously, has been a common practice in calculating the axial force demand of columns, per capacity design principles (Bruneau et al. 2011). While current design procedures [such as those prescribed by the AISC 341-10 (AISC 2010) Seismic Design Provisions 2010] consider simultaneous story yielding at all stories, studies have shown that, though this can occur for low-rise structures, it is not necessarily the case for mid- to high-rise structures (Redwood and Channagiri 1991; Tremblay and Robert 2001; Lacerte and Tremblay 2006; Richards 2009; Bruneau et al. 2011). Hence, this practice overestimates axial force demand, which can, in the case of tall structures, result in large, uneconomical column sections. Nonlinear time history analysis using a large number of earthquakes can be conducted to establish axial force demand in columns of a given structure. However, such analysis is typically done after design, for verification purposes only, and is not a preferred design approach.

A number of researchers have conducted studies on axial force demand in columns and its estimation. Redwood and Channagiri (1991) proposed that the axial force in a column at a particular level could be obtained by adding the vertical component of the brace forces immediately above that story to the square root of sum of squares (SRSS) of vertical forces from all the other braces above that level. However, Tremblay and Robert (2001) showed that the application of this method yielded results similar to those obtained by the capacity design method at upper levels, but nonconservative results at lower levels of low- and mid-rise chevron-braced frames when compared with results from nonlinear time history analyses. Lacerte and Tremblay (2006) proposed a method that considered the forces in critical braces as 1.0 and 1.2 times the expected brace capacity in tension and compression, respectively, and brace forces in all the other floors as those obtained when brace buckling initiates in these stories (provided the resulting column axial force is not less than that obtained from the combination of expected brace capacity in tension and postbuckling residual compression strength in compression, over all stories). For eight- and twelve-story structures, this approach showed satisfactory results over the building height when compared with results from nonlinear time history analyses, but was conservative for the four-story structure considered. Richards (2009) investigated the demands on seismic columns of various types of braced frames, considering four different system strengths and three different structural heights. It was observed that the overstrength factor, Ω_0, of 2 used in designing those frames was nonconservative in many cases but conservative at the base of tall structures, and that assuming simultaneous yielding over the entire height of tall buildings was overly conservative. These studies were empirical, relying on nonlinear time history analysis of a number of typical frames. While these studies have provided valuable insights regarding seismic demand in columns, a systematic and generalized way to estimate these column forces is desirable.

A different approach, investigated by the authors, considered the estimation of the number of simultaneously yielding stories,

[1]Structural Engineer, Earthquake Engineering Research and Consultation Center, Kathmandu, Nepal (corresponding author). Email: lisashre4@gmail.com

[2]Professor, Dept. of Civil, Structural, and Environmental Engineering, Univ. at Buffalo, State Univ. of New York, Buffalo, NY 14260. Email: bruneau@buffalo.edu

Note. This manuscript was submitted on July 15, 2017; approved on January 19, 2018; published online on June 20, 2018. Discussion period open until November 20, 2018; separate discussions must be submitted for individual papers. This paper is part of the ***Journal of Structural Engineering***, © ASCE, ISSN 0733-9445.

N_{SYS}, as the key to finding the axial force demand in columns. In order to develop a systematic procedure for estimating the number of simultaneously yielding stories and to use it to find axial force demand in columns of buildings subjected to ground excitation (other than by empirically analyzing a large number of archetype structures), and focusing on shear-type buildings initially for simplicity, three essential steps were envisioned: (1) a procedure had to be developed for estimating the number of simultaneously yielding stories in a simple shear building subjected to velocity-pulse base excitation; (2) this procedure had to be adapted for shear buildings subjected to actual earthquake excitations, taking the perspective that earthquakes can be represented as a series of pulses, and; (3) a procedure had to be formulated to estimate the axial force demand in columns considering the force transferred from the simultaneously yielding stories and the other nonyielded stories above the column under consideration.

Accordingly, Shrestha and Bruneau (2017b) proposed a procedure to estimate the number of simultaneously yielding stories in a shear-type building subjected to full-sine velocity-pulse base excitation. Full-sine velocity-pulse base excitation was considered from the perspective that an earthquake can be represented by a series of such pulses. In that paper, concepts of wave propagation were used to find the number of simultaneously yielding stories. An estimation method was proposed, based on the observation that story yielding is dependent on the magnitude of the velocity wave propagating along the building height, and it was found to provide a good estimate of the actual N_{SYS} values. In Shrestha and Bruneau (2017a), the aforementioned estimation procedure was used to estimate the N_{SYS} values in a shear building subjected to earthquake-base excitation by identifying and representing the main pulse of an earthquake velocity record responsible for causing the maximum number of stories to yield simultaneously by a full-sine pulse. Overall, the estimated N_{SYS} values were satisfactorily close to the actual values, with the estimated values being on the conservative side. Note that wave propagation along the height of a building has been used previously for other purposes. For example, Hall et al. (1995), Safak (1999), Humar (2002), Clough and Penzien (2003), Krishnan and Muto (2012) used this approach to find or understand the response of structures to pulses and earthquakes; similarly, Snieder and Safak (2006), Todorovska and Trifunac (2008a), Todorovska and Trifunac (2008b), Todorovska and Rahmani (2013), and Ebrahimian and Todorovska (2014) used it for system identification and health monitoring purposes, although all of these studies assumed elastic structural response.

This paper focuses on the third of the aforementioned steps. Using the procedure presented by Shrestha and Bruneau (2017a) to determine the number of simultaneously yielding stories due to an earthquake-base excitation, a procedure is proposed to estimate the axial force demands at various stories of shear-type frame structures. Although buckling-restrained braces (BRBs) are used in the analyses, for the analyses conducted, degrees of freedom are restrained so as to impose shear-type deformations to the frame.

The study conducted by the authors was to investigate if the code prescribed axial force to be considered in column design can be modified by relaxing the number of stories yielding simultaneously as it can become quite a conservative requirement in tall structures. The study presented here focused on initial steps towards establishing an estimation procedure that can eventually be used to reduce such specified seismic column force demands in codes and specifications. The estimation procedure proposed here is an approximate approach; however, the study showed that the proposed procedure could yield good estimates of the number of simultaneously yielding stories and axial force demand in columns for the earthquakes and structures considered, with the estimated values generally being on the conservative side. Further studies of the effectiveness of the proposed procedure using different types of structures and archetypes are foreseen in the future, but the information presented here provides the basis for such studies and can be improved upon by further research.

Analysis Parameters

Structural System

This study considered a forty-story shear-type structure. A buckling restrained brace frame was used, with degree of freedom restrained so as to enforce shear-type behavior. The BRB frame was designed such that the inelastic response is concentrated only in the braces; the beam and column members are designed to remain elastic. The beams and braces are connected to the columns through pin connections. The shear yield capacity, V_p, of the brace at each floor of the BRB frame structure was chosen to be equal to the story shear capacity at the corresponding floor of the shear building model with varying story stiffness over building height (Structure-IV) used in Shrestha and Bruneau (2017a). Note that the distribution of shear yield capacity over the height of that structure was based on the lateral force distribution prescribed by code (see Shrestha and Bruneau 2016, 2017b for definition). A response reduction factor R (the ratio of the maximum elastic shear force demand of a story to the shear yield capacity of that story) of 8 was selected for the strength of the base story. Note that in the analysis, to obtain R of 8 at the base, the ground motion was scaled up by 7.48 (for details on calculating the scale of the ground motion needed to obtain R of 8, see Shrestha and Bruneau 2016). However, the force reduction factor will not necessarily be equal to 8 at the other stories. The ratio of lateral stiffness of column k_{col} to lateral stiffness of brace k_{br} at each story was chosen to be 0.25 for most of the analyses, but the value of that ratio was varied in some analyses to assess the sensitivity of the results to variations in that parameter.

Input Excitation

The study considered three categories of input earthquake excitations, namely: (1) earthquake excitations having a single dominant pulse in their velocity record (Category A), (2) earthquake excitations having multiple distinct pulses in their velocity record (Category B), and (3) earthquake excitations that do not have distinct pulses in their velocity record (i.e., non-pulse type earthquake velocity excitations; Category C). Six earthquakes were considered for each category, resulting in the 18 earthquakes shown in Table 1. Since many of the earthquakes considered have large duration pulses, the structural response is affected by overlaps of the numerous reflected waves with long wavelengths generated at the boundaries of the structure. Thus, in addition to the analyses performed using the original ground motions, analyses were also carried out with a condensed time scale of the acceleration records to understand the effects of the incident wave and the overlaps of the incident and reflected waves that occur at the top and base of the structure. The condensed base excitations used by Shrestha and Bruneau (2017a) to obtain a $0.5t_d{:}t_H$ value equal to 0.4, where, t_d denotes the duration of the main pulse of the velocity record, and t_H denotes the time taken by the wave to travel through the height of the building, were also used here. Note that the extent over which the first half of a pulse spans over the height of a building is measured by the $0.5t_d{:}t_H$ ratio. If $0.5t_d{:}t_H$ is greater than 1, the first half of the pulse extends beyond the height of the building, and if it is less than 1, it spans over only some stories. Also note that, because the BRB frames considered here have different

Table 1. Earthquake ground motions considered

Category	Number	Earthquake	Identifier	Station	M_w	PGA (g)	PGV (cm/s)	PGD (cm)
A	1	1994 Northridge	WPI046	Newhall-W.Pico Canyon Rd.	6.7	0.455	92.8	56.64
	2	1992 Landers	LCN275	Lucerne	7.3	0.785	31.9	16.42
	3	1979 Imperial Valley	H-E04230	El Centro Array #4	6.5	0.36	76.6	59.02
	4	1987 Superstition Hills (B)	B-PTS225	5051 Parachute Test Site	6.7	0.455	112	52.8
	5	1999 Chi Chi, Taiwan	TCU068-N	TCU068	7.6	0.462	263.1	430
	6	1999 Chi Chi,Taiwan	CHY101-N	CHY101	7.6	0.44	115	68.75
B	7	1999 Duzce, Turkey	DZC270	Duzce	7.1	0.535	83.5	51.59
	8	1999 Kocaili, Turkey	YPT060	Yarimca	7.4	0.349	62.1	50.97
	9	1994 Northridge	CNP196	Canoga Park-Topanga Canyon	6.7	0.42	60.8	20.17
	10	1989 Loma Prieta	HAD255	1656 Hollister Diff. Array	6.9	0.279	35.6	13.05
	11	1994 Northridge	RO3090	90006 Sun Valley-Roscoe Blvd.	6.7	0.443	38.2	10.04
	12	1984 Morgan Hill	CYC285	57217 Coyote Lake Dam (SW Abut)	6.2	1.298	80.8	9.63
C	13	1966 Parkfield	C12320	1016 Cholame #12	6.1	0.063	6.8	3.55
	14	1952 Kern County	HOL090	135 LA Hollywood Stor FF	7.4	0.044	6	2.77
	15	1957 San Francisco	GGP100	1117 Golden Gate Park	5.3	0.112	4.6	0.43
	16	1971 San Fernando	ORR021	24278 Castaic—Old Ridge Route	6.6	0.324	15.6	2.31
	17	1940 Imperial Valley	I-ELC180	117 El Centro Array #9	7	0.313	29.8	13.32
	18	1949 Western Washington State	49OLY	Olympia Test Laboratory	6.5	0.206	16	4.19

Note: PGA = peak ground acceleration; PGV = peak ground velocity; and PGD = peak ground displacement.

Table 2. Ratios of t_d:T_n and t_d:$2t_H$ for the BRB frames subjected to earthquake-base excitation

Serial number	Earthquake	Original time scale					Condensed time scale				
		t_d (s)	t_H (s)	$0.5t_d$:t_H	T_n (s)	t_d:T_n	t_d (s)	t_H (s)	$0.5t_d$:t_H	T_n (s)	t_d:T_n
1	WPI046	2.53	0.43	2.96	1.35	1.88	0.81	0.84	0.48	2.65	0.31
2	LCN275	4.59	0.42	5.43	1.33	3.44	0.82	1.41	0.29	4.44	0.18
3	H-E04230	4.35	0.44	4.92	1.39	3.12	0.81	1.33	0.3	4.19	0.19
4	B-PTS225	2.23	0.42	2.66	1.32	1.69	0.81	0.82	0.5	2.57	0.32
5	TCU068-N	10.93	0.47	11.68	1.48	7.41	0.81	1.24	0.33	3.92	0.21
6	CHY101-N	5.54	0.44	6.32	1.38	4.01	0.81	1.4	0.29	4.43	0.18
7	DZC270	4.1	0.49	4.16	1.56	2.64	0.81	1.32	0.31	4.17	0.19
8	YPT060	3.53	0.42	4.25	1.31	2.69	0.81	1.16	0.35	3.65	0.22
9	CNP196	2.08	0.54	1.91	1.72	1.21	0.81	1.1	0.37	3.47	0.23
10	HAD255	2.66	0.59	2.24	1.87	1.42	0.81	1.56	0.26	4.91	0.16
11	RO3090	1.06	0.69	0.77	2.18	0.49	0.81	0.88	0.46	2.77	0.29
12	CYC285	1.01	0.62	0.82	1.95	0.52	0.81	0.64	0.63	2.03	0.4
13	C12320	3.32	1.49	1.11	4.71	0.7	0.81	3.37	0.12	10.64	0.08
14	HOL090	2.92	1.17	1.25	3.69	0.79	0.81	4.06	0.1	12.82	0.06
15	GGP100	0.45	2.93	0.08	9.26	0.05	0.81	1.77	0.23	5.57	0.14
16	ORR021	0.97	1.48	0.33	4.66	0.21	0.81	1.59	0.26	5.01	0.16
17	I-ELC180	2.47	0.73	1.69	2.3	1.07	0.81	1.83	0.22	5.76	0.14
18	49OLY	2	0.85	1.17	2.69	0.74	0.81	1.7	0.24	5.35	0.15

story stiffness than the shear building model (Structure-IV) used previously, the corresponding t_H value (which depends on story stiffness value) will be different. Hence, $0.5t_d$:t_H values will also be different than 0.4. The resulting $0.5t_d$:t_H and t_d:T_n ratios for the BRB frames subjected to original and condensed time scale are shown in Table 2. Here, T_n denotes the time period of the frames.

OpenSees Model

This study used the OpenSees analysis software (version 2.4.3) for the numerical analyses of the BRB frames considered. The columns were modeled using elastic beam–column elements and the beams were modeled using elastic truss elements. The braces were modeled using truss elements that undergo inelastic deformation. A bilinear elastic-ideal-plastic model was used. In order to avoid numerical error, a strain hardening ratio r of 1% with a kinematic strain hardening hysteretic model was adopted (note that the effect of more significant values of strain hardening on response is investigated in a subsequent subsection). Rayleigh damping with viscous damping of 2% defined at the first and twenty-fourth modes was considered. In order to impose shear-building type behavior on the structure, the joints where the columns and beams meet were restrained against rotation and vertical translation, and the horizontal translation at the ends of the beam were constrained to be equal.

Estimating the Number of Simultaneously Yielding Stories in BRB Frames

Estimation Procedure

The procedure used here for estimating the number of simultaneously yielding stories in a BRB frame subjected to an earthquake excitation involves idealizing the main pulse of the velocity record

of the earthquake with an equivalent full-sine pulse (Shrestha and Bruneau 2016, 2017a). To summarize, the steps required to find the number of simultaneously yielding stories are explained as follows:

1. Calculate the minimum magnitude of the velocity wave v_y required to yield a story for all the stories of the frame. For the BRB frames considered here, if shear stiffness and shear yield capacity of the brace member at a particular story, with mass $\bar{m}$ and height h, are denoted by k_{br} and $V_{p,br}$, respectively, the v_y values of the stories can be calculated using Eq. (1) (see Shrestha and Bruneau 2016, 2017b):

$$v_y = \frac{V_{p,br}\left(1 + \frac{k_{col}}{k_{br}}\right)}{\sqrt{\bar{m}h(k_{col} + k_{br})}} \tag{1}$$

2. Find the candidates for the main pulse in the velocity record by finding the pulses in the velocity record corresponding to the N_C peaks/troughs that have the largest amplitudes in their displacement record. Here, N_C is the number of candidate pulses to be considered. There is a direct relationship between the velocity base excitation and the story forces (Shrestha and Bruneau 2016, 2017b). Hall et al. (1995), Dicleli and Bruneau (1995), and Krishnan and Muto (2012) have also indicated the importance of velocity ground excitation in the response of a structure. Hence, velocity records are considered when choosing the main pulse responsible for causing the maximum number of stories to yield simultaneously.
3. Once the v_y values of all the stories and the candidate pulses are known, identify the main pulse of the velocity earthquake record by comparing the nw_{avg} product for each candidate pulse. Here, n is the number of stories that have v_y values lower than the amplitude of the first half of the pulse, and w_{avg} is the average width of first half of the candidate velocity pulse below the highest v_y value or the peak of the candidate velocity pulse, whichever is larger. To find the maximum number of simultaneously yielding stories, a pulse with magnitude higher than the v_y values of most of the stories and a width that can span over the maximum number of stories of a building is required. Hence, consideration of the area of the portion of a pulse below the maximum v_y values of the stories is more significant than the entire area of the pulse. The proposed procedure for identifying the main pulse of the velocity record is based on these criteria and is described in more detail in Shrestha and Bruneau (2016, 2017a).
4. Idealize the main pulse of the velocity record with a full-sine pulse by (1) considering the time period of the idealized pulse to make it equal to that of the actual main pulse of the earthquake record, and (2) setting the amplitude of the idealized pulse equal to the average of the amplitude of the first and second halves of the main pulse of the actual record. The idea of representing ground motions either by equivalent pulses, series of equivalent pulses, or dominant pulses has been around for decades. Techniques for representing near-fault pulses vary, from the use of simple pulses like rectangular, triangular, and trigonometric (sine, cosine) functions [as considered in Hall et al. (1995) and Bruneau and Wang (1996a, b), etc.] to more advanced techniques that use wavelet analysis [studied by Mavroeidis and Papageorgiou (2003), Baker (2007), and Vissiliou and Makris (2011)]. Here, a simple approach was adopted, since the use of a simple full-sine pulse for idealizing this main pulse was observed in many instances to be sufficient for the intended purpose. Simple pulse models, such as the sinusoidal pulses used by Kalkan and Kunnath (2006), the triangular wave trains used by Krishnan and Muto (2012), and other similar simple pulses, have been reported adequate to satisfactorily capture the salient responses of structures.
5. Once the main pulse is idealized with a full-sine velocity pulse, find the estimated number of simultaneously yielding stories due to the incident wave, $N_{SYS,Incident}$, by adopting the procedure proposed for full-sine velocity-pulse base excitation in Shrestha and Bruneau (2016, 2017b). In that procedure, the equations derived for t_C and t_D curves, which define the predicted beginning and end of story yielding, are used to obtain the $N_{SYS,Incident}$ value. Two methods for estimating the number of simultaneously yielding stories caused by full-sine base excitations were proposed: (1) considering the actual shape of the base excitation, and (2) assuming the shape of the velocity pulse to be a rectangular pulse. In this study, the first approach has been adopted because it was shown to give better results; the second approach, while having the benefit of providing a closed-form solution, gives more conservative results.
6. To estimate the axial force demand in the columns at different floors of the building, both simultaneously yielding stories due to the incident wave and simultaneous story yielding due to the constructive overlaps of the velocity waves at the top and base of the building should be considered. For the sake of expediency, find the number of simultaneously yielding stories due to constructive overlaps of the velocity waves at the top ($N_{SYS,Top}$) and bottom ($N_{SYS,Base}$) of the building by considering it to be equal to the number of stories within the span of the overlap with v_y values less than $2v_{g0}$, where v_{g0} is the amplitude of the idealized main pulse of the earthquake velocity record (Shrestha and Bruneau 2016, 2017a).

Estimation Results

Condensed Time Scale

Fig. 1 shows the time history of brace yielding and the number of simultaneously yielding stories obtained from the OpenSees analysis results and the estimation procedure for shear-type BRB frames subjected to some of the representative earthquake excitations with condensed acceleration time scale. The figure shows brace yielding in the positive and negative directions at various times throughout the response as observed from the OpenSees analysis results. Since short time intervals are considered here, the dots in the figure overlap and look like horizontal bars. Hence, the length of the bars corresponds to the duration of yielding. As the wave propagates, brace yielding progresses along the height. The t_C and t_D curves that represent the predicted beginning and end of brace yielding are also shown. The t_C and t_D curves adequately envelop the story yielding caused by the main pulse of the earthquake excitation. Time histories of the total number of simultaneously yielding stories (1) observed from the OpenSees analysis for the positive and negative yielding caused by the actual earthquake, and (2) obtained using the aforementioned estimation procedure are also shown in the figure. The results show that the estimated numbers of simultaneously yielding stories due to the incident wave $N_{SYS,Incident}$ are satisfactorily close to the actual values observed from the OpenSees analysis results. Note that, in this figure and other similar figures, different time scales have been used deliberately to highlight the time window where prominent yielding occurred for each earthquake.

To estimate the axial force demand in the columns, the maximum number of simultaneously yielding stories when the incident wave travels to the top of the building is considered and is denoted by $MN_{SYS,Incident}$. The estimated number of simultaneously yielding stories due to the incident wave and due to overlapping of the waves—i.e., the $MN_{SYS,Incident}$, $N_{SYS,Top}$, and $N_{SYS,Base}$ values—obtained for each of the ground motions considered are shown in

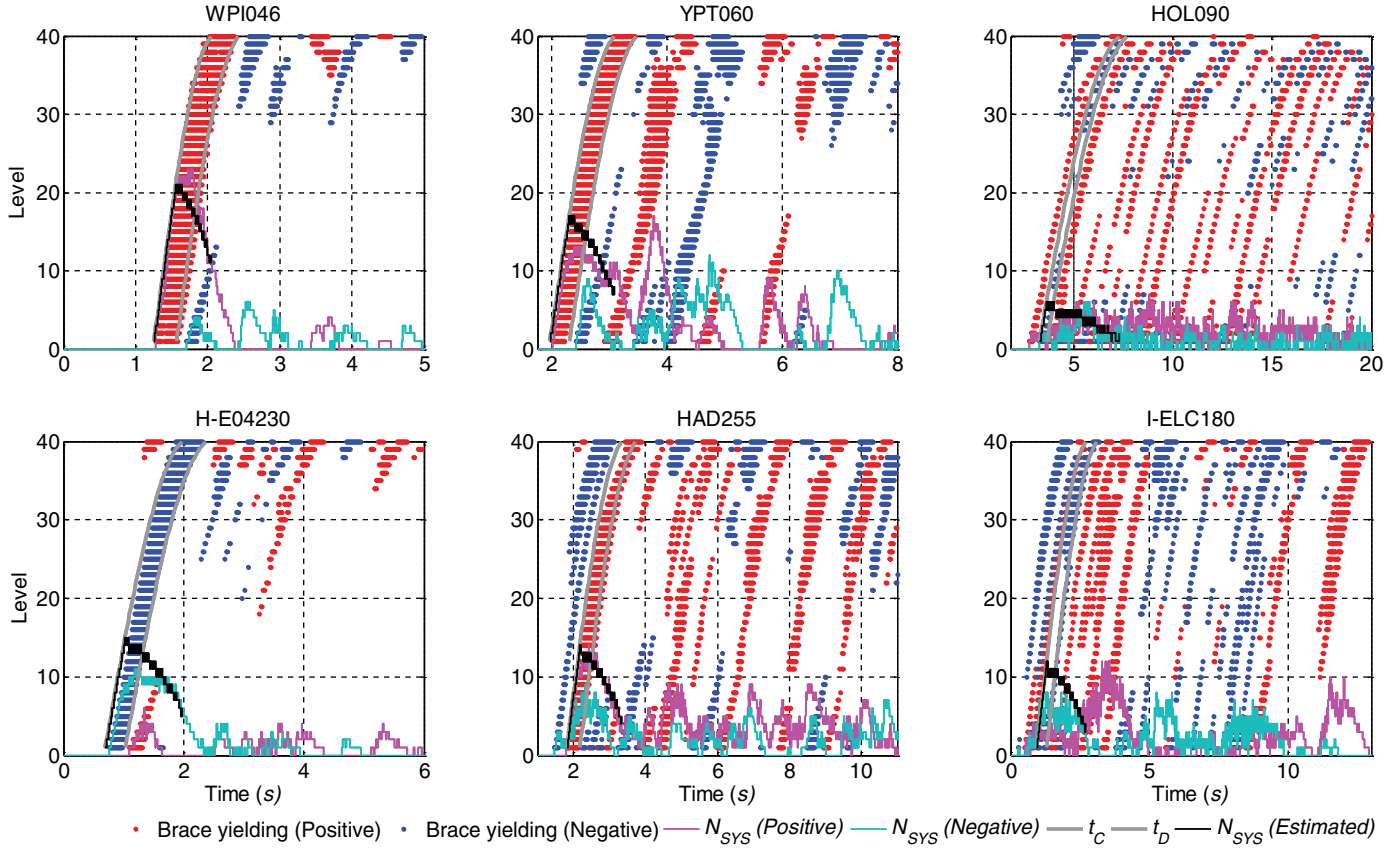

Fig. 1. Actual and estimated time history of brace yielding and number of simultaneously yielding stories (N_{SYS}) of shear-type BRB frame subjected to earthquake excitations with condensed acceleration time scale.

Table 3. The table shows the maximum number of simultaneously yielding stories obtained from the estimation procedure (i.e., maximum of $MN_{SYS,Incident}$, $N_{SYS,Top}$, and $N_{SYS,Base}$) and the actual values obtained from the OpenSees analysis results; for comparison, the table also shows the discrepancies between the two values, expressed as percentages. These discrepancies are shown for all the earthquake cases considered in order to provide insight into how the estimation procedure works for each of the earthquakes considered.

On average, for all the earthquakes, the discrepancy between the estimated and the actual N_{SYS} value is 17.82%, as shown in Table 4; the predicted results are generally on the conservative side.

Table 3. Estimated and actual number of simultaneously yielding stories for shear-type BRB frames subjected to earthquakes with condensed time scale

Serial number	Earthquake	$0.5t_d$:t_H	Estimated			Maximum N_{SYS}		Discrepancy (%)
			$MN_{SYS,Incident}$ (full-sine)	$N_{SYS,Top}$	$N_{SYS,Base}$	Estimated	Actual	
1	WPI046	0.48	21	13	13	21	23	−8.7
2	LCN275	0.29	15	5	8	15	11	36.36
3	H-E04230	0.3	15	6	8	15	11	36.36
4	B-PTS225	0.5	22	13	13	22	15	46.67
5	TCU068-N	0.33	16	7	9	16	10	60
6	CHY101-N	0.29	14	5	8	14	8	75
7	DZC270	0.31	15	6	8	15	9	66.67
8	YPT060	0.35	17	7	9	17	17	0
9	CNP196	0.37	17	8	10	17	13	30.77
10	HAD255	0.26	14	5	7	14	14	0
11	RO3090	0.46	19	12	12	19	32	−40.63
12	CYC285	0.63	27	19	17	27	24	12.5
13	C12320	0.12	7	1	3	7	7	0
14	HOL090	0.1	6	1	2	6	7	−14.29
15	GGP100	0.23	12	4	6	12	12	0
16	ORR021	0.26	13	4	7	13	15	−13.33
17	I-ELC180	0.22	12	3	6	12	12	0
18	49OLY	0.24	12	4	6	12	9	33.33

Table 4. Average and standard deviation of the discrepancy between the estimated and actual number of simultaneously yielding stories for shear-type BRB frames subjected to earthquakes with condensed time scale

Earthquakes considered	Average (%)	Standard deviation (%)
All earthquakes	17.82	31.71
Categories A and B earthquakes only	26.25	34.45

The standard deviation for the discrepancy is 31.71%. Since the estimation procedure is not expected to work as accurately for Category C earthquakes as it did for Category A and B earthquakes, the table also shows the average and standard deviation of the discrepancy for the twelve earthquakes belonging to Categories A and B. The average discrepancy between the estimated and actual maximum N_{SYS} for the first twelve earthquakes is 26.25%, with a standard deviation of 34.45%. When only Categories A and B earthquakes are considered, the average discrepancy is greater than when all three earthquake categories are considered. The greater discrepancy between the estimated and actual number of yielding stories for Categories A and B earthquakes occurs when a greater number of stories yield; this reflects the fact that the results are more sensitive to earthquakes having larger pulses, which is not unreasonable from the perspective of seismic inelastic response.

Original Time Scale

Results for the shear-type BRB frame subjected to the original (i.e., unmodified time scale) earthquakes are shown in Fig. 2. Note that only representative earthquakes are shown in the figure; results for all the earthquakes are shown in Shrestha and Bruneau (2016). The main pulse of most of the original earthquake excitations has long pulse duration in their velocity record. The $0.5t_d$:t_H value for these 18 earthquakes varies between 0.08 and 11.68, with an average of 2.99 (see Table 2). The figures show that for most of the cases with $0.5t_d$:t_H values larger than 1, the t_C curve accurately indicates the beginning of the story yields, but the t_D curve does not match well with the end of the story yields. The story yield durations observed, in general, are shorter than the estimated durations. This is due to the overlapping of the incident and reflected waves of the large duration velocity pulses. For example, in case of the WPI046 earthquake record, when the incident wave reaches the top of the building, only the first third of the half-sine velocity pulse spans over the building height (approximately). As the next third enters the building, the reflected velocity wave (with opposite sign) generated at the top of the building moves down, decreasing the drift caused by the incident wave. Thus, the actual yield duration is shorter than the duration obtained from the estimation procedure. The response of the building and hence the yield patterns, are the results of the overlaps of the incident wave and numerous reflected waves with large wavelength generated every time a wave hits the boundary of the structure. For some of the earthquake records, namely H-E04230, TCU068-N, YPT060, CNP196, and CYC285, actual story yielding occurs later than what was predicted by the t_C curve. This is due to the smaller values (coordinates) of the main pulse of the actual velocity record compared to the idealized pulse at the beginning of the pulse, and also due to the decrease in the drift caused by the overlapping (combined effects) of the incident and numerous reflected waves of the long-duration main pulse.

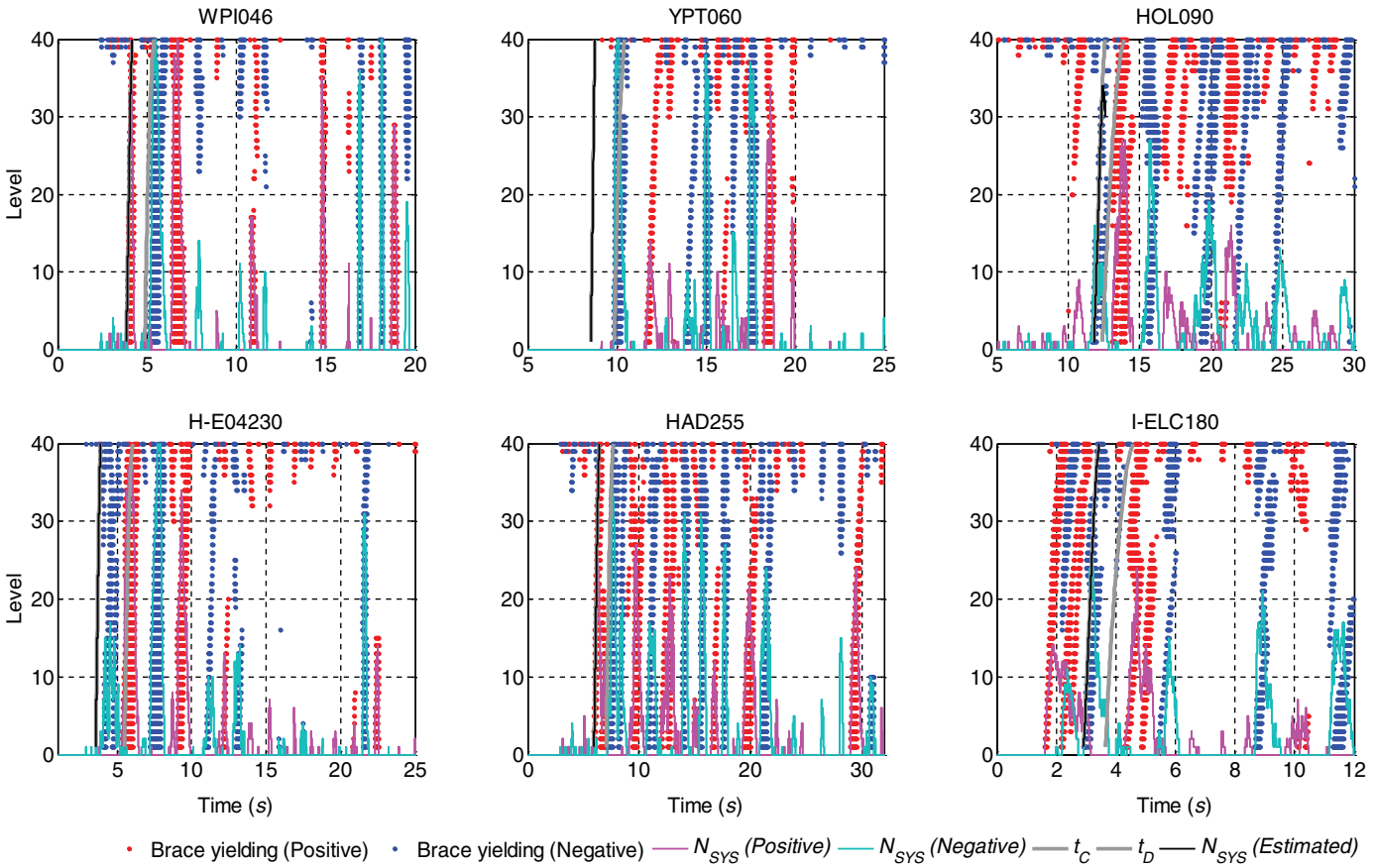

Fig. 2. Actual and estimated time history of brace yielding and number of simultaneously yielding stories (N_{SYS}) of shear-type BRB frame subjected to original earthquake excitations.

Table 5. Estimated and actual number of simultaneously yielding stories for shear-type BRB frames subjected to earthquakes with original time scale

Serial number	Earthquake	$0.5t_d$:t_H	Estimated			Maximum N_{SYS}		Discrepancy (%)
			$MN_{SYS,Incident}$ (Full-sine)	$N_{SYS,Top}$	$N_{SYS,Base}$	Estimated	Actual	
1	WPI046	2.96	40	40	40	40	40	0
2	LCN275	5.43	40	40	40	40	37	8.11
3	H-E04230	4.92	40	40	40	40	40	0
4	B-PTS225	2.66	40	40	40	40	40	0
5	TCU068-N	11.68	40	40	40	40	40	0
6	CHY101-N	6.32	40	40	40	40	40	0
7	DZC270	4.16	40	40	40	40	40	0
8	YPT060	4.25	40	40	40	40	40	0
9	CNP196	1.91	40	40	39	40	37	8.11
10	HAD255	2.24	40	40	40	40	36	11.11
11	RO3090	0.77	29	26	20	29	40	−27.5
12	CYC285	0.82	33	29	22	33	25	32
13	C12320	1.11	38	40	28	40	33	21.21
14	HOL090	1.25	34	40	31	40	27	48.15
15	GGP100	0.08	5	0	2	5	6	−16.67
16	ORR021	0.33	16	7	9	16	15	6.67
17	I-ELC180	1.69	40	40	37	40	24	66.67
18	49OLY	1.17	38	40	29	40	31	29.03

Overall, when the pulses had a $0.5t_d$:t_H value larger than 1, the earthquakes caused simultaneous yielding over all of the stories; such simultaneous yielding over the entire height did not happen for the RO3090, CYC285, GGP100, and ORR021 earthquake records, which all had a $0.5t_d$:t_H value less than 1. For most of the original earthquakes considered here, the $0.5t_d$:t_H ratio was greater than 1, likely causing all the stories in the building to yield simultaneously. However, these earthquakes may not necessarily result in $0.5t_d$:t_H greater than 1 for other structures; the $0.5t_d$:t_H ratio may be greater than or less than 1, in other cases, depending on the properties of the building. For structures that have a $0.5t_d$:t_H ratio less than 1, the estimation procedure will provide a more accurate estimation of N_{SYS} value and axial force demand in the columns than estimations obtained from code procedures. Hence, to investigate the number of simultaneously yielding stories for structures that have a $0.5t_d$:t_H ratio less than 1, another set of earthquakes was considered by reducing the time scale of the original earthquakes.

Table 5 presents the estimated and actual number of simultaneously yielding stories, along with the discrepancy between the two values, obtained for shear-type BRB frames subjected to earthquakes with original time scale. On average, considering all eighteen earthquakes, the maximum estimated N_{SYS} is 10.38% more than the actual value, with a standard deviation of 22.32% as shown in Table 6. The average discrepancy between the estimated and actual maximum N_{SYS} for the first twelve earthquakes (Categories A and B) is 2.65%, with a standard deviation of 13.32%. The average discrepancy is smaller when only earthquake Categories A and B are considered than when all three earthquake categories are considered. The earthquakes belonging to Categories A and B have long-duration pulses capable of producing yield over nearly the entire height of the structure; hence, the results saturate and the discrepancy attenuates.

Table 6. Average and standard deviation of the discrepancy between the estimated and actual number of simultaneously yielding stories for shear-type BRB frames subjected to earthquakes with original time scale

Earthquakes considered	Average (%)	Standard deviation (%)
All earthquakes	10.38	22.32
Categories A and B earthquakes only	2.65	13.32

Estimating Axial Force Demand in the Columns

Estimation Procedure

Once the number of simultaneous stories yielding due to the incident wave and overlapping at the top and base (i.e., $MN_{SYS,Incident}$, $N_{SYS,Top}$, and $N_{SYS,Base}$ values) are obtained, the axial force induced at a particular column is calculated individually for the three cases by considering the force transferred from the simultaneously yielding stories and the square root of sum of squares of the vertical force transferred by relevant braces considering their yield capacity. The estimated axial force demand ($P_{Estimated}$) in a particular column is given by the maximum value resulting from the three cases. The procedures for estimating the axial force demand for each of the three cases are explained below.

Axial Force Demand due to Simultaneous Yielding Caused by the Incident Wave

The axial force demand at a particular story of the building due to the incident wave, $P_{Incident}$, can be obtained by developing a procedure to account for contributions to axial force coming from stories with braces that have yielded and from those with braces that have not yielded. The first part of this procedure consists of summing up the vertical force transferred to the column by the $MN_{SYS,Incident}$ stories that have yielded. The $MN_{SYS,Incident}$ simultaneously yielding stories are considered to consist of the column whose axial force demand is to be determined and $MN_{SYS,Incident} - 1$ stories directly above it. The second part of that procedure consists of the vertical forces coming from the remaining braces above, that may or may not be close to yielding, but have not yielded. To account for this contribution, SRSS of the vertical force component of these braces' yield strength is added as a proposed approach.

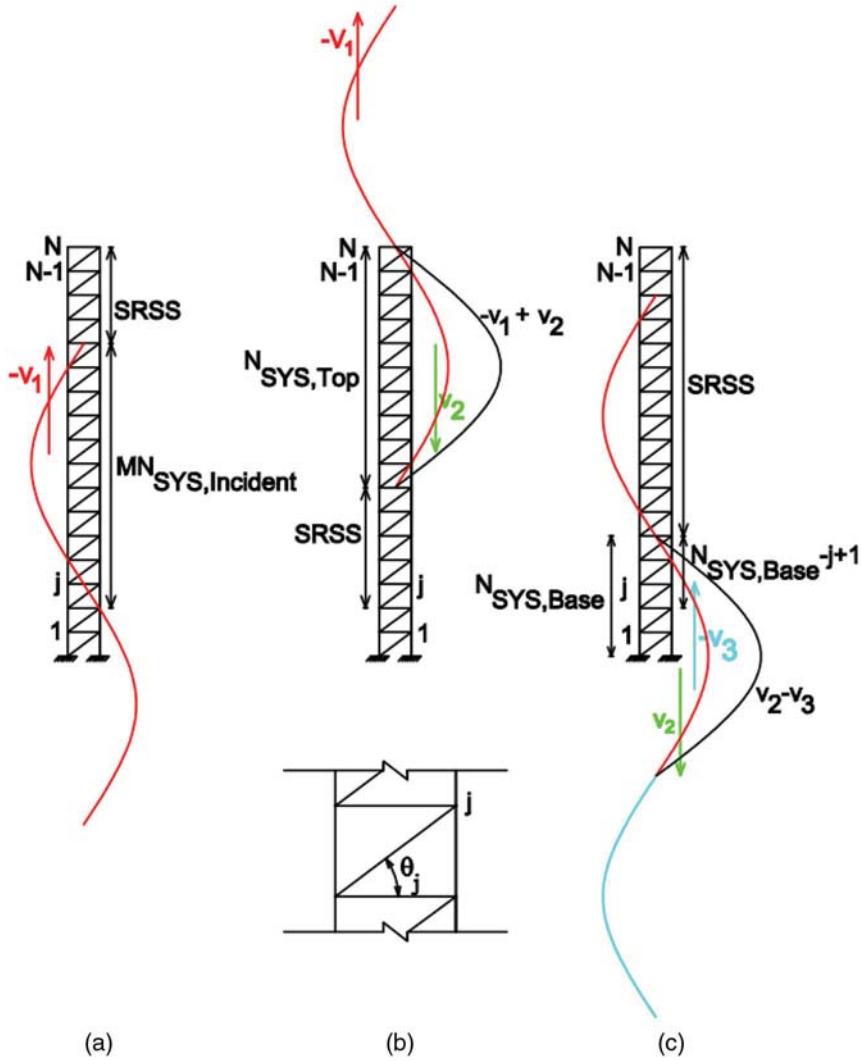

Fig. 3. Axial force demand at *j*th story due to the simultaneous yielding of stories caused by (a) incident wave; (b) overlap at the top; and (c) overlap at the base.

Fig. 3(a) illustrates schematically the range of stories for each part of this procedure to find the axial force demand in the column at the *j*th floor due to the simultaneous yielding of the stories caused by the incident wave and SRSS of the remaining stories above level *j*. Eq. (2) provides the corresponding expressions for calculating the axial force demand in the *j*th column for the incident wave case denoted by $P_{Incident,j}$. Eq. (2*a*) is for the case when the column under consideration has more than or equal to $MN_{SYS,Incident}$ stories above it. The axial force demand in the column is due to the vertical force from the $MN_{SYS,Incident}$ simultaneously yielding stories, including the story under consideration and the remaining $MN_{SYS,Incident} - 1$ directly above it, and SRSS of the vertical force (considering the full yield capacity) from the remaining (not yielding) stories above it. Eq. (2*b*) is for the case when the column under consideration has less than $MN_{SYS,Incident}$ stories above it. The axial force demand in the column, in this case, is due to the vertical force from simultaneously yielding stories, including the story under consideration, and the remaining stories directly above it

$$P_{Incident,j} = \sum_{i=j}^{j+MN_{SYS,Incident}-1} f_y A_{br,i} \sin\theta_i + \sqrt{\sum_{i=j+MN_{SYS,Incident}}^{N} (f_y A_{br,i} \mathrm{Sin}\theta_i)^2} \qquad \text{for } j \le N - MN_{SYS,Incident} \tag{2a}$$

$$P_{Incident,j} = \sum_{i=j}^{N} f_y A_{br,i} \sin\theta_i \qquad \text{for } j > N - MN_{SYS,Incident} \tag{2b}$$

where f_y = yield stress for the steel material considered; $A_{br,I}$ = area of the brace at the *i*th floor; θ_i = angle of inclination (with the horizontal) of the brace member at the *i*th story as shown in Fig. 3(b); and N = total number of stories in the building.

Axial Force Demand due to Simultaneous Yielding Caused by Constructive Overlapping at the Top

To consider the possibility that wave overlap at the top of the frame may govern the demand in a much lower story j, the vertical force transferred to the jth column from braces at the topmost $N_{SYS,Top}$ stories (i.e., the stories within the overlap region) are summed up. Then, the SRSS of the vertical forces corresponding to the yield strength of the braces for the story under consideration and rest of the stories above that story is added to the axial demand at story j. Fig. 3(b) schematically illustrates the range of stories for each part of this procedure and Eq. (3) provides the corresponding expression for finding the axial force demand in the column at the jth floor, denoted by $P_{Top,j}$, for the case of overlapping of the waves at the top of the building. Eq. (3*a*) is for the case when the column under consideration has more than or equal to $N_{SYS,Top}$ stories above it. The axial force demand in the column is due to the vertical force from the $N_{SYS,Top}$ simultaneously yielding stories at the top of the building, and SRSS of the vertical force (considering the full yield capacity) from the story under consideration and the remaining (not yielding) stories above it. Eq. (3*b*) is for the case when the column under consideration has less than $N_{SYS,Top}$ stories above it (i.e., for columns that fall within the span of the overlap). The axial force demand in the column in this case is due to the vertical force from the simultaneously yielding stories, including the story under consideration and the remaining stories above it

$$P_{Top,j} = \sum_{i=N-N_{SYS,Top}+1}^{N} f_y A_{br,i} \sin\theta_i + \sqrt{\sum_{i=j}^{N-N_{SYS,Top}} (f_y A_{br,i} \mathrm{Sin}\theta_i)^2} \qquad \text{for } j \le N - N_{SYS,Top} \tag{3a}$$

$$P_{Top,j} = \sum_{i=j}^{N} f_y A_{br,i} \sin\theta_i \qquad \text{for } j > N - N_{SYS,Top} \tag{3b}$$

Axial Force Demand due to Simultaneous Yielding Caused by Constructive Overlapping at the Base

Similarly, to consider the possibility that maximum demand in story j may occur after the passage of the reflected wave, the vertical force transferred to the column by the braces in the $N_{SYS,Base}$ stories at the base of the building (i.e., the stories within the overlap region) are summed up. The SRSS of the vertical force transferred from rest of the braces above that story are then added, considering their full yield capacity. Fig. 3(c) schematically illustrates the range of stories for each part of this procedure, while Eq. 4 provides the corresponding expression to calculate the axial force demand at the jth column, denoted by $P_{Bottom,j}$, caused by the overlapping of the velocity waves at the base of the building. Eq. (4*a*) is for the case when the column under consideration has less than $N_{SYS,Bottom}$ stories below it (i.e. for columns that fall within the span of the overlap). The axial force demand in the column is due to the vertical force from the simultaneously yielding stories, including the story under consideration, and remaining $N_{SYS,Bottom} - j$ stories directly above it, and SRSS of the vertical force, considering the full yield capacity, from the remaining (not yielding) stories above the column under consideration. Eq. (4*b*) is for the case when the column under consideration has more than $N_{SYS,Bottom}$ stories below it. The axial force demand in the column is given by the SRSS of the vertical force (considering the full yield capacity) of the column under consideration and the remaining stories above it

$$P_{Bottom,j} = \sum_{i=j}^{N_{SYS,Bottom}} f_y A_{br,i} \sin\theta_i + \sqrt{\sum_{i=N_{SYS,Bottom}+1}^{N} (f_y A_{br,i} \mathrm{Sin}\theta_i)^2} \qquad \text{for } j \le N_{SYS,Bottom} \tag{4a}$$

$$P_{Bottom,j} = \sqrt{\sum_{i=j}^{N} (f_y A_{br,i} \mathrm{Sin}\theta_i)^2} \qquad \text{for } j > N_{SYS,Bottom} \tag{4b}$$

Estimation Results

Fig. 4 shows the axial force time history obtained from the OpenSees analyses at the columns of some of the selected stories in a shear-type BRB frame subjected to the 1994 Northridge (WPI046) earthquake record with condensed time scale. The figure also shows the estimated axial force demand obtained by considering simultaneous story yielding due to the incident wave ($P_{Incident}$), due to the overlapping of the waves at the top (P_{Top}), and due to the overlapping at the base (P_{Base}) of the building using the equations presented in the previous section. Comparisons of the actual axial force in the column versus the estimated values show that the estimation procedure gives a good estimate of the actual axial force demand. Note that the axial force demand due to the incident wave dominates.

In order to compare the actual axial force demand in the column to the estimated values and to assess the adequacy of the estimation procedure more efficiently, Figs. 5 and 6 show the ratios of the estimated axial force due to the incident wave ($P_{Incident}$), overlap at the top (P_{Top}), and overlap at the base (P_{Base}), to the maximum axial force demand from OpenSees analysis (P_{Actual}) at different stories of the BRB frame for earthquakes with condensed and original time scale, respectively. The figures also show the average of $P_{Estimated}$:P_{Actual} values at different stories of the BRB.

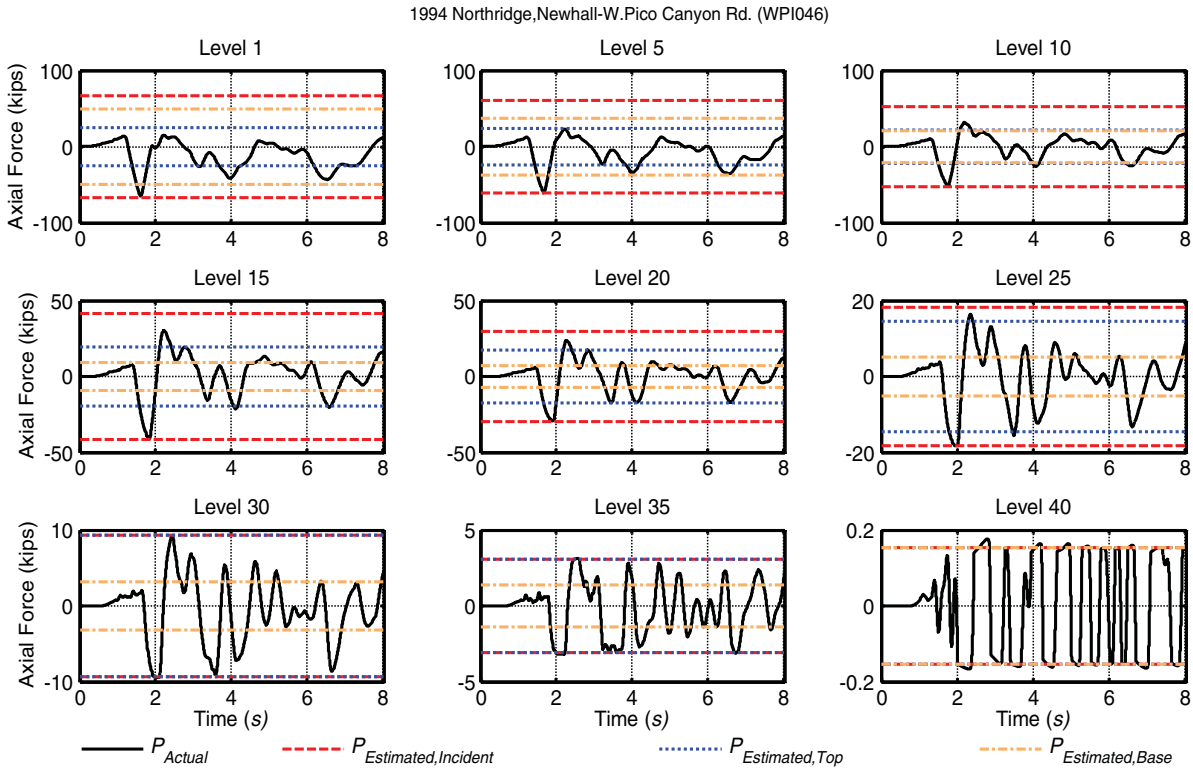

Fig. 4. Time history of the actual and estimated axial force demand at the columns of some selected stories of a shear-type BRB frame subjected to 1994 Northridge, Newhall-W.Pico Canyon Rd. (WPI046) earthquake record with condensed time scale.

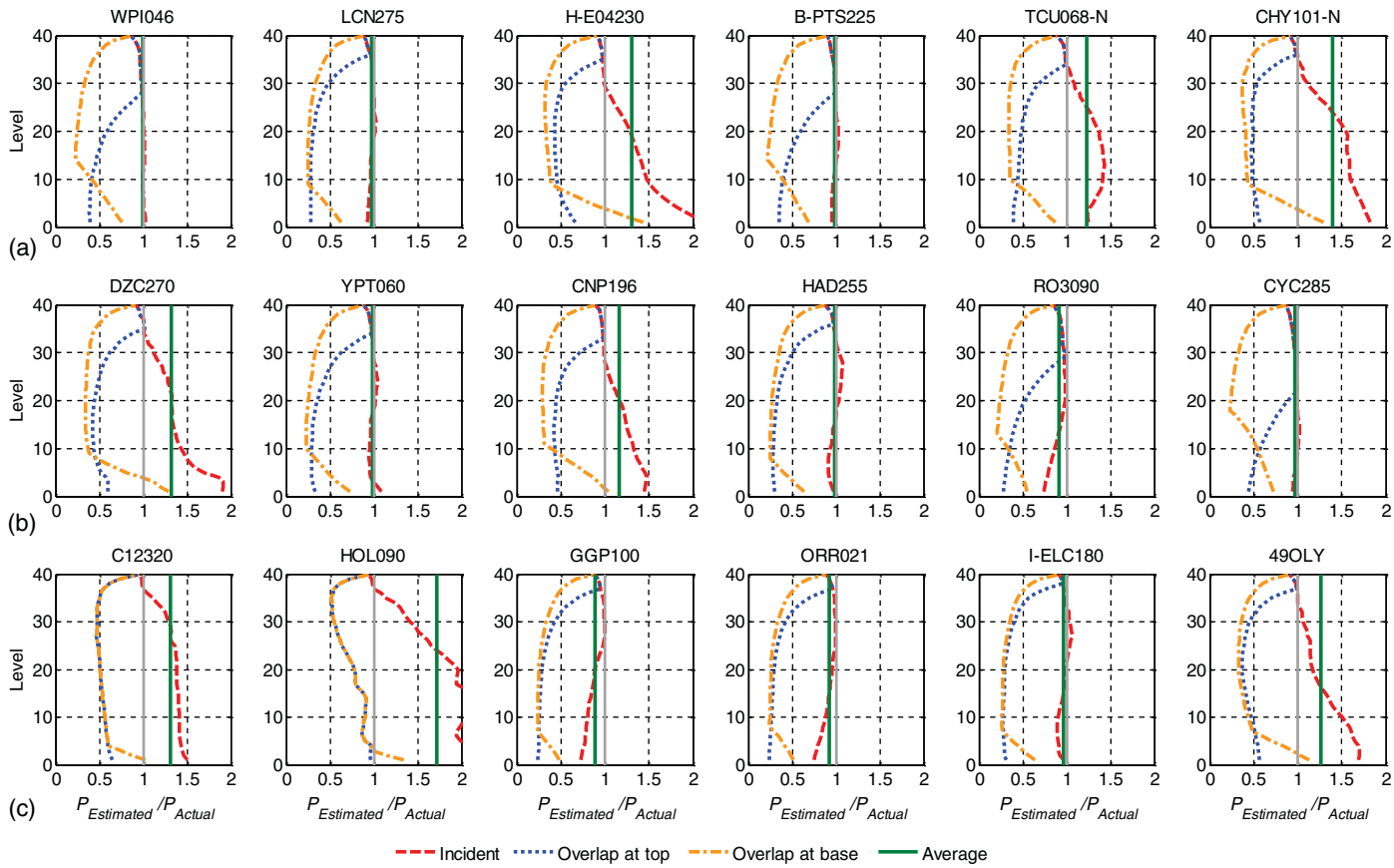

Fig. 5. Ratio of estimated to actual axial force demand in columns at different stories of the shear-type BRB frame subjected to earthquakes of (a) Category A; (b) Category B; and (c) Category C, with condensed acceleration time scale.

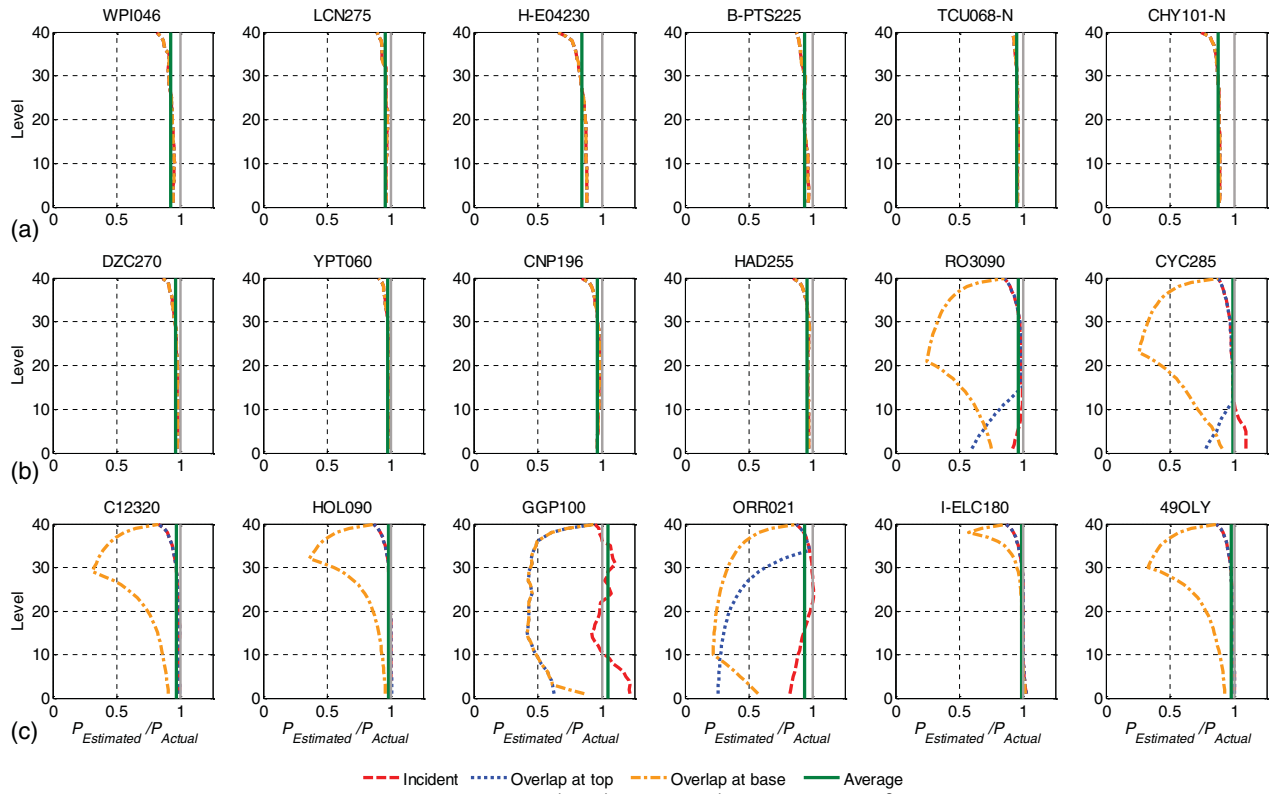

Fig. 6. Ratio of estimated to actual axial force demand in columns at different stories of the shear-type BRB frame subjected to earthquakes of (a) Category A; (b) Category B; and (c) Category C, with original acceleration time scale.

Condensed Time Scale

Plots of $P_{Estimated}$:P_{Actual} for a shear-type building subjected to earthquakes with condensed time scale, in Fig. 5, show that the axial force demand obtained using the incident wave typically dominates. The estimated axial force closely matched the actual axial demand for almost half of the earthquakes, namely WPI046, LCN275, B-PTS225, YPT060, HAD255, CYC285, and I-ELC180. For three earthquakes, RO3090, GGP100, and ORR021, the estimation procedure underestimated values at the lower stories. For rest of the earthquakes, mainly nonpulse type earthquakes, the estimation procedure gave significantly overestimated values. The average $P_{Estimated}$:P_{Actual} for the shear-type BRB frame for all 18 earthquakes was 1.12. In other words, on average, the column axial force obtained from the estimation procedure was 12% more than the actual values. In the upper few stories, the procedure gave slightly underestimated values. This was due to the strain hardening in the upper stories that yield significantly due to the constructive overlapping of the waves. This effect has not been taken into account in the estimation procedure; therefore, it may explain the discrepancy between the two results.

Original Time Scale

In the case of original earthquake records (Fig. 6), most of the earthquake records had $0.5t_d$:t_H value much greater than 1; thus, the first part of the main pulse covers the entire building height and simultaneous yielding occurs over all the stories. The axial force demand estimated considering the incident wave alone, overlapping at the top, and overlapping at the base, in most of the cases, were found to yield the same results. Overall, the estimation procedure slightly underestimated the axial force demands. This is due to the strain hardening of the yielded braces in the actual model, which is not considered in the estimation procedure. Even though the strain hardening provided was negligible, the small increment in axial forces beyond yield capacity occurring at simultaneously yielding stories added up and created the discrepancy noted. Overall, the estimated axial force demand was 4.7% less than the actual axial force demands.

Parametric Study

The analysis of the BRB frames performed so far considered that columns provided a lateral story stiffness of 0.25 times that of braces, while elastic-ideal-plastic material properties were considered for the braces. In order to understand how the results (in terms of story yield pattern, actual and estimated number of simultaneously yielding stories, and actual and estimated axial force demands in the columns) would change for BRB frames having a k_{col}:k_{br} ratio other than 0.25, or how they would change when braces having strain hardening instead of elastic-ideal-plastic material behavior were used, sensitivity analyses were performed by varying these two parameters. For this purpose, k_{col}:k_{br} ratios ranging from 0.01 to 1 and strain hardening ratios varying from 1 to 12.5% were considered. For the sake of expediency, only three of the eighteen earthquake ground motions were used—namely 1994 Northridge, Newhall-W.Pico Canyon Rd. (WPI046); 1999 Kocaili, Yarimca (YPT060); and 1952 Kern County, LA Hollywood Stor FF (HOL090)—to represent earthquakes belonging to Categories A, B, and C, respectively, with both original and condensed time scale.

Effects of Column Stiffness

To study the effects of column stiffness on the response of shear-type BRB frames and on the results obtained from the estimation procedure, k_{col}:k_{br} values of 0.01, 0.1, 0.25, 0.5, 0.75, and 1.0 were

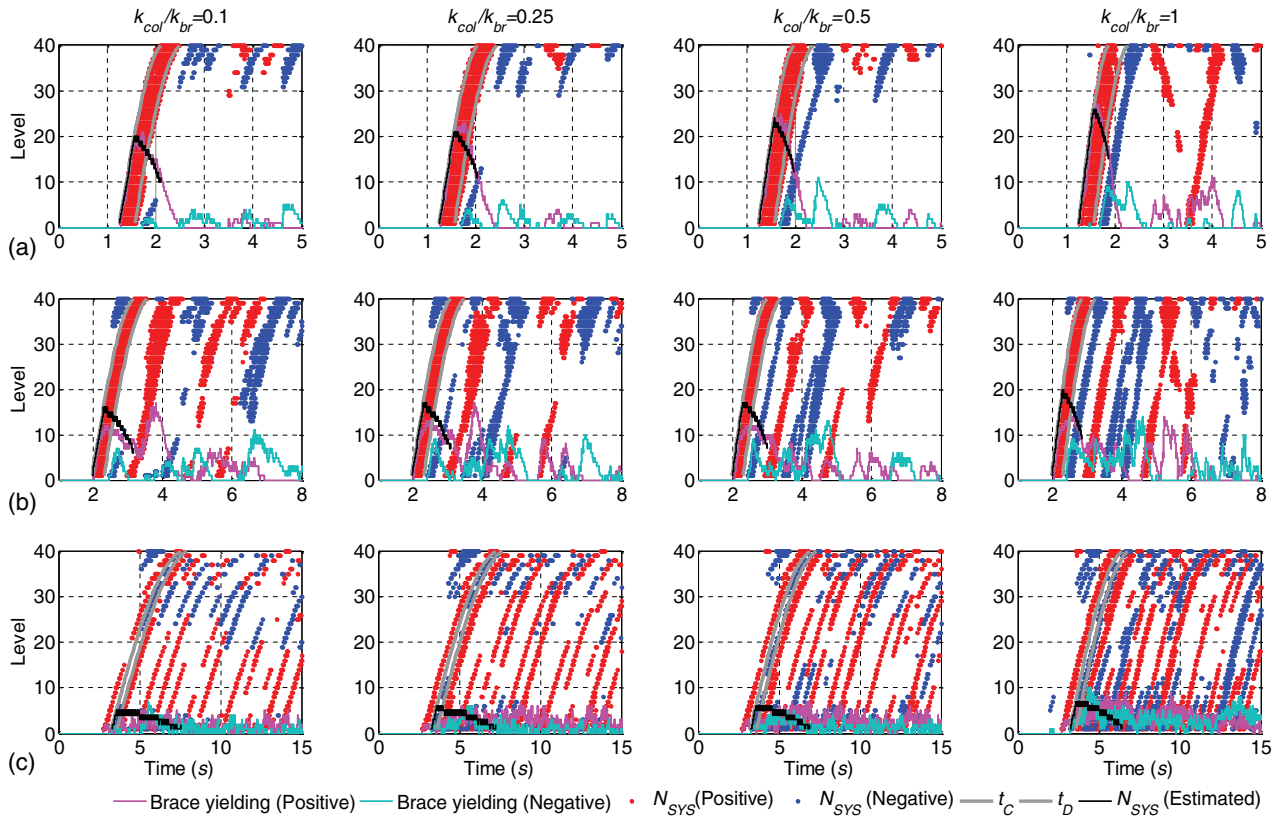

Fig. 7. Actual and estimated time history of brace yielding and number of simultaneously yielding stories (N_{SYS}) of shear-type BRB frames with different k_{col}:k_{br} values, subjected to (a) 1994 Northridge, Newhall-W.Pico Canyon Rd.; (b) 1999 Kocaili, Yarimca; and (c) 1952 Kern County, LA Hollywood Stor FF earthquake records with condensed time scale.

considered. The same shear-type BRB frames described in the previous section "Structural System" have been used, but with different column stiffness.

Condensed Time Scale

Fig. 7 shows the story yielding pattern and number of simultaneously yielding stories obtained from OpenSees analysis results and from the estimation procedure for the three earthquakes representing the three categories of earthquakes. Due to space limitations, results for only four values of stiffness ratios are shown, k_{col}:k_{br} values of 0.1, 0.25, 0.5, and 1.0 (see Shrestha and Bruneau (2016) for results for all k_{col}:k_{br} values). The t_C and t_D curves estimated well the beginning and end of story yielding due to the first part of the main pulse in the case of the 1994 Northridge, Newhall-W.Pico Canyon Rd. (WPI046) earthquake and the 1999 Kocaili, Yarimca (YPT060) earthquake [Figs. 7(a and b), respectively], which represent the first two categories of earthquakes. The estimated maximum number of simultaneously yielding stories was found to be close to the actual values obtained from the OpenSees analysis. Thus, the axial force demand estimated using the idealized main pulse was close to the actual demand indicated by $P_{Estimated}$:P_{Actual} values close to 1.0 at most of the stories, as shown in Fig. 8, which presents the results for the axial force demands. The axial force demand estimated using the incident wave dominated.

As explained previously, for the 1952 Kern County, LA Hollywood Stor FF (HOL090) record—which represents the third category of earthquakes [Fig. 7(c)]—there is interference in the response of the individual pulses due to the closely spaced high frequency pulses in the velocity record. The story yielding due to the incident wave of the main pulse did not occur as predicted by the t_C and t_D curves at many stories. The estimation procedure was found to provide conservative results when estimating the N_{SYS} values and when estimating the axial force demand as indicated by the $P_{Estimated}$:P_{Actual} values. However, with increases in the k_{col}:k_{br} value, actual and estimated story yielding matched more closely; hence, the estimated axial force demands in the columns were found to be closer to the actual values.

As stiffness increases, the wave velocity increases; thus, as k_{col}:k_{br} increases, the velocity wave reaches the top earlier, as marked by the beginning of yielding at the top story and the increase in the slope of the yield pattern. Also, with increases in wave velocity, the time required for the wave to pass through the building height t_H decreases and the $0.5t_d$:t_H ratio increases. Therefore, with increases in k_{col}:k_{br} ratio, the number of simultaneously yielding stories increases.

Original Time Scale

Fig. 9 shows the story yield pattern along with the N_{SYS} values while Fig. 10 shows the $P_{Estimated}$:P_{Actual} for the BRB frames with different k_{col}:k_{br} values, again subjected to the aforementioned three earthquakes, but this time with original time scale. Due to the large duration of the velocity pulse of the earthquake record, estimated and actual simultaneous yielding occured over all stories of the building for all the k_{col}:k_{br} values considered, except for the third earthquake with lower k_{col}:k_{br} ratios. For the first two earthquakes, the number of times the story yielding occurred increased with increase in column stiffness. However, variation in column stiffness did not seem to cause any other significant difference in estimating the number of simultaneously yielding stories and in the axial force demand in columns, because the earthquakes

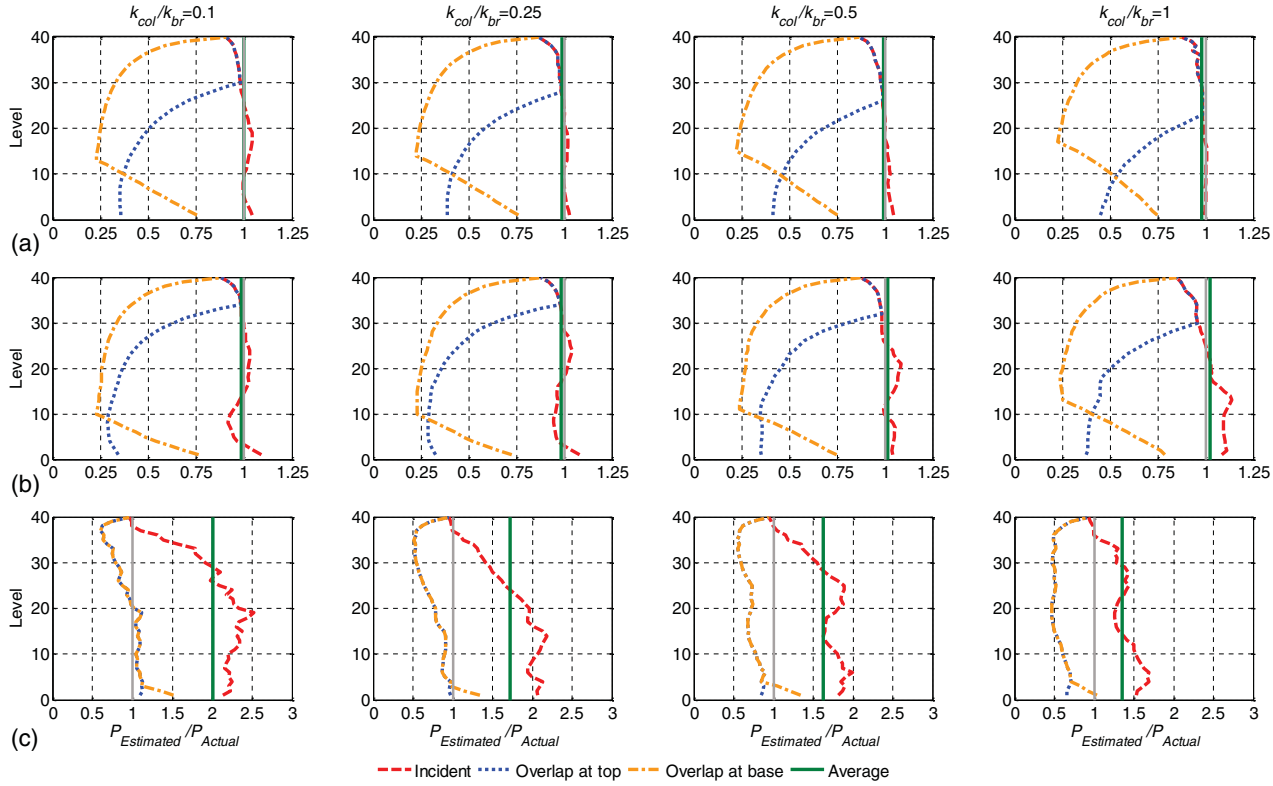

Fig. 8. Ratio of estimated to actual axial force demand in columns of shear-type BRB frames with different k_{col}:k_{br} values, subjected to (a) 1994 Northridge, Newhall-W.Pico Canyon Rd.; (b) 1999 Kocaili, Yarimca; and (c) 1952 Kern County, LA Hollywood Stor FF earthquake records with condensed time scale.

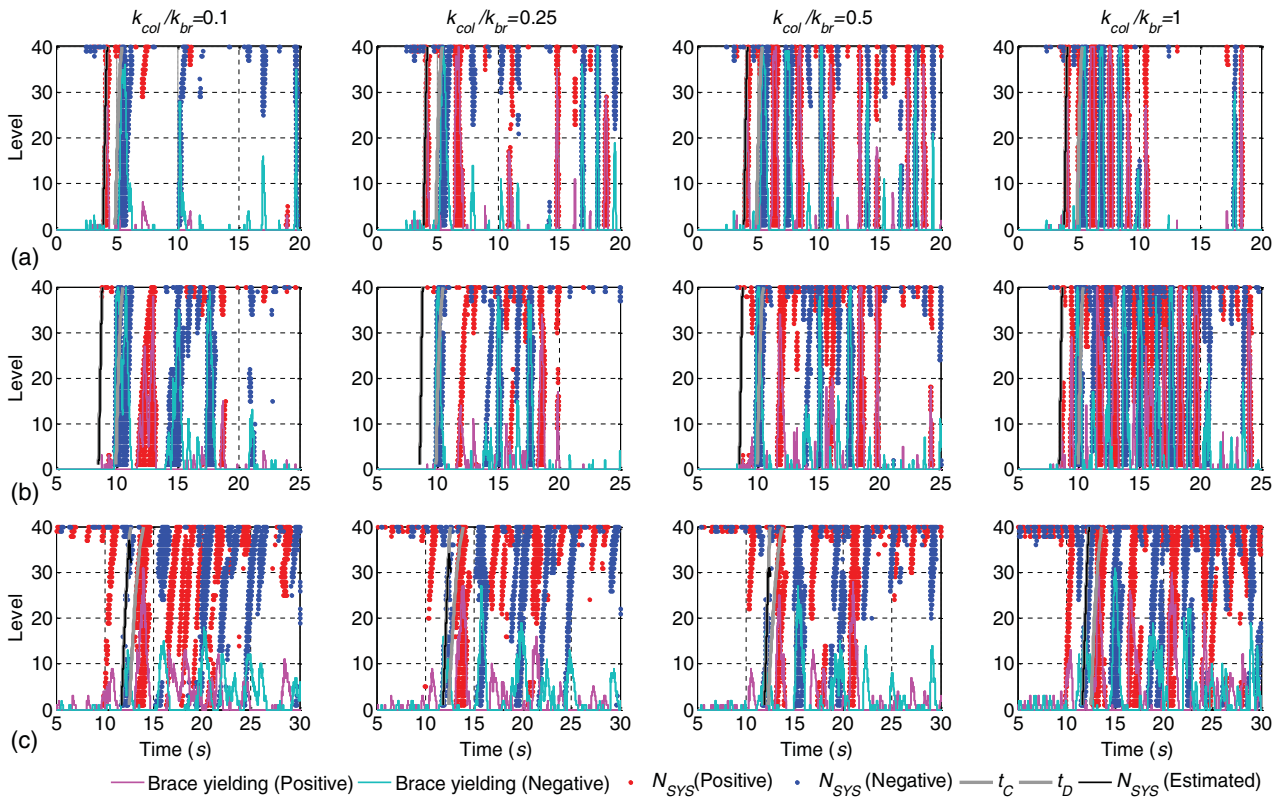

Fig. 9. Actual and estimated time history of brace yielding and number of simultaneously yielding stories (N_{SYS}) of shear-type BRB frames with different k_{col}:k_{br} values, subjected to (a) 1994 Northridge, Newhall-W.Pico Canyon Rd.; (b) 1999 Kocaili, Yarimca; and (c) 1952 Kern County, LA Hollywood Stor FF earthquake records with original time scale.

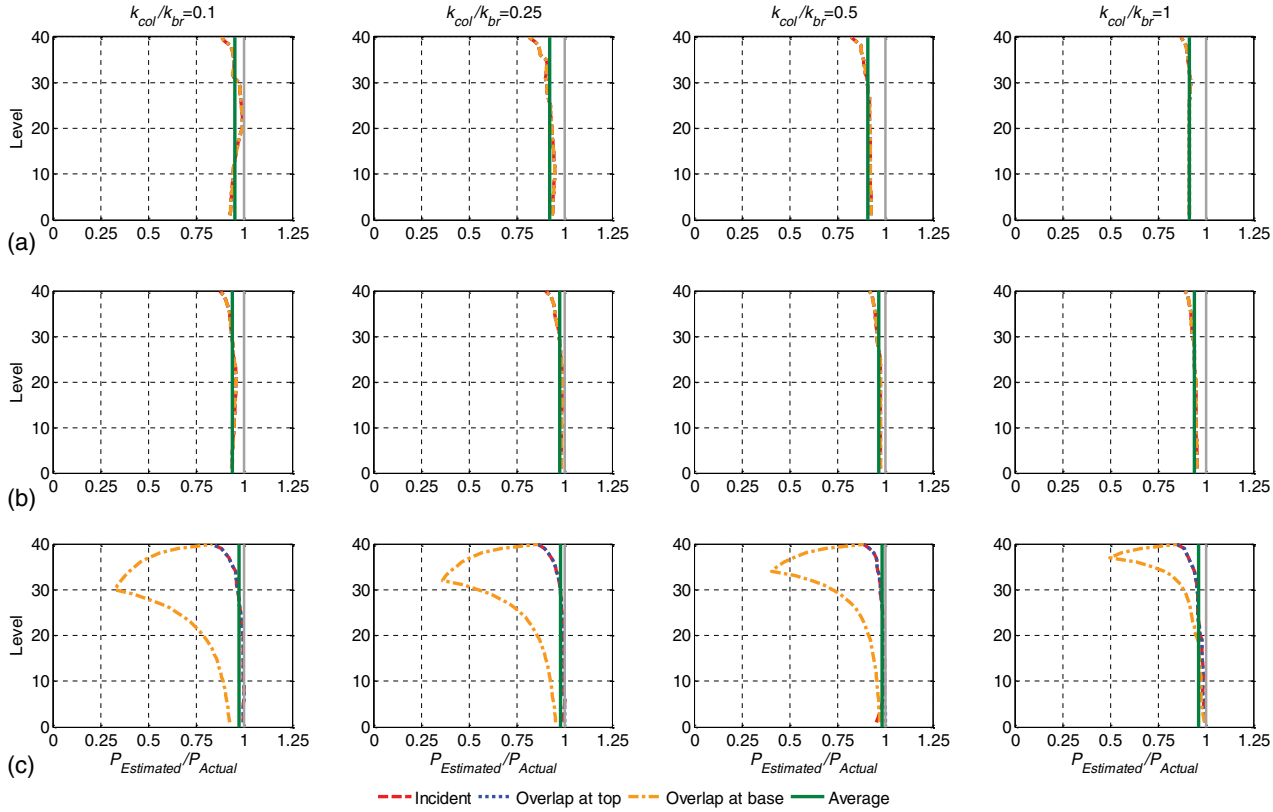

Fig. 10. Ratio of estimated to actual axial force demand in columns of shear-type BRB frames with different k_{col}:k_{br} values, subjected to (a) 1994 Northridge, Newhall-W.Pico Canyon Rd.; (b) 1999 Kocaili, Yarimca; and (c) 1952 Kern County, LA Hollywood Stor FF earthquake records with original time scale.

involved long-duration pulses and simultaneously yielded all the stories. The estimated axial force demand due to the simultaneous story yielding caused by the incident wave, overlapping at the top, and overlapping at the base yield the same results except for the 1952 Kern County, LA Hollywood Stor FF (HOL090) earthquake record. At the upper stories, the estimation procedure underestimated the axial force demands, due to the strain hardening effect that was not considered in the estimation procedure, as explained previously.

Effects of Strain Hardening Ratio

To investigate the application of the estimation procedures for finding the number of simultaneously yielding stories and axial force demand in columns for structures with strain hardening, OpenSees analyses of shear-type BRB frames with braces having a strain hardening ratio r with values of 1.0, 2.5, 5.0, 7.5, 10, and 12.5% were conducted. The same shear-type BRB frame described in the section "Structural System" was used; only the strain hardening ratio was changed.

Condensed Time Scale

Fig. 11 shows the story yield pattern, t_C and t_D curves, and the number of simultaneously yielding stories for the three earthquake cases with condensed time scale. Due to space limitations, only the results for the strain hardening ratios of 1.0, 2.5, 7.5, and 12.5% are shown [see Shrestha and Bruneau (2016) for results for all the strain hardening ratios]. For the first two earthquakes, the procedure for estimating the number of simultaneously yielding stories using the idealized main pulse of the velocity record of an earthquake proposed in this research worked well, as can be seen by comparing the yield duration predicted by the t_C and t_D curves against the actual yielding from OpenSees analysis results, and also by comparing estimated and actual N_{SYS}. For the third earthquake, some of the stories did not yield as predicted by the t_C and t_D curves; thus, the estimated N_{SYS} due to the incident wave of the main pulse does not match the actual value.

Fig. 12 shows $P_{Estimated}$:P_{Actual} values at different stories for different strain hardening ratios and earthquake excitations with condensed time scale. As strain hardening ratio increases, $P_{Estimated}$:P_{Actual} values decrease. This is logical, because the estimation procedure does not consider strain hardening (i.e., the estimated axial force remains the same for all strain hardening cases considered, whereas the actual axial force increases with increases in strain hardening). Thus, the proposed procedure for finding the axial force demand in columns underestimates the force that develops in the frame when strain hardening braces are considered. One exception is the third earthquake case, for which the estimation procedure is found to provide quite conservative results for all the strain hardening ratios considered.

Original Time Scale

For large duration pulses, the increase in strain hardening ratio does not create much difference in the estimation of N_{SYS} values (Fig. 13), since yielding occurs, regardless of strain hardening ratio, over all of the building stories. However, while finding axial force demand, as strain hardening increases, $P_{Estimated}$:P_{Actual} values decrease (Fig. 14); this is due to the fact that strain hardening is not considered in calculating the value of $P_{Estimated}$ (which remains the same, regardless of strain hardening) whereas the P_{Actual} value increases with increases in strain hardening, as explained previously.

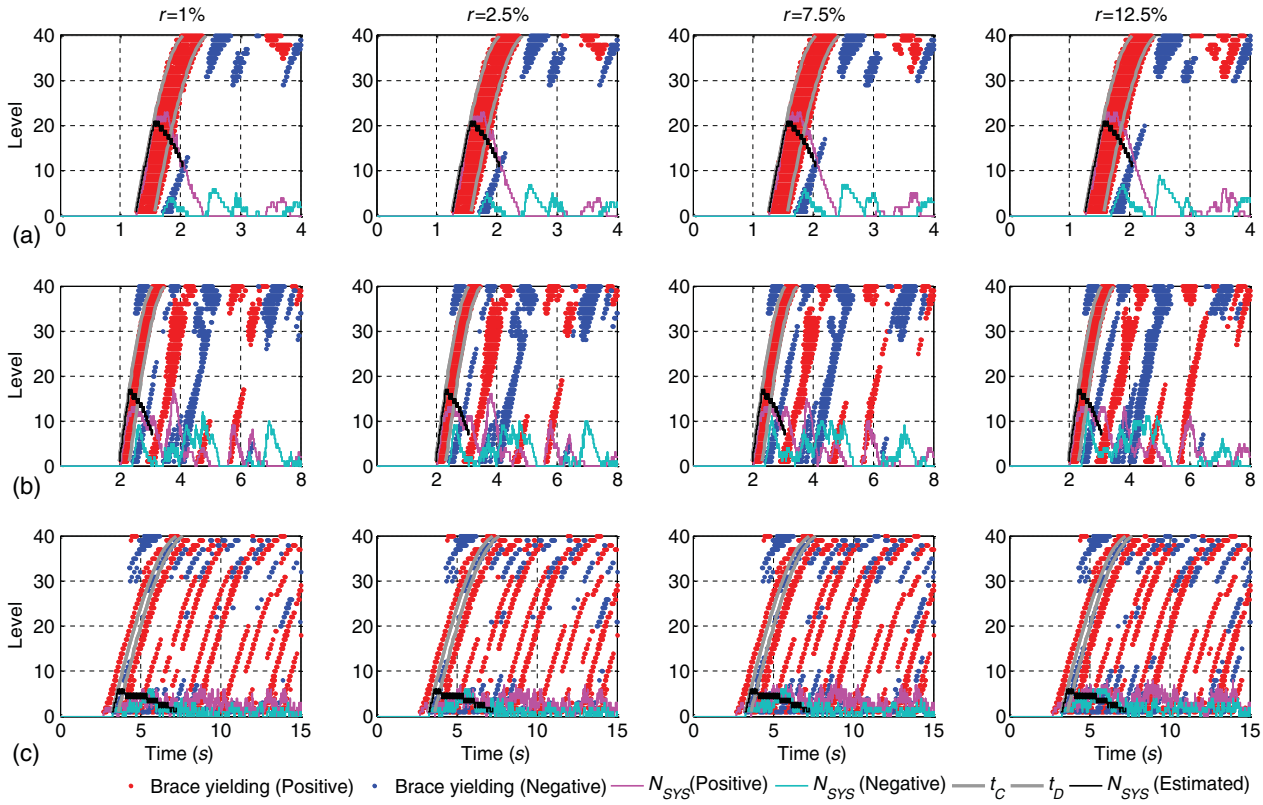

Fig. 11. Actual and estimated time history of brace yielding and number of simultaneously yielding stories (N_{SYS}) of shear-type BRB frames with different strain hardening ratios, subjected to (a) 1994 Northridge, Newhall-W.Pico Canyon Rd.; (b) 1999 Kocaili, Yarimca; and (c) 1952 Kern County, LA Hollywood Stor FF earthquake records with condensed time scale.

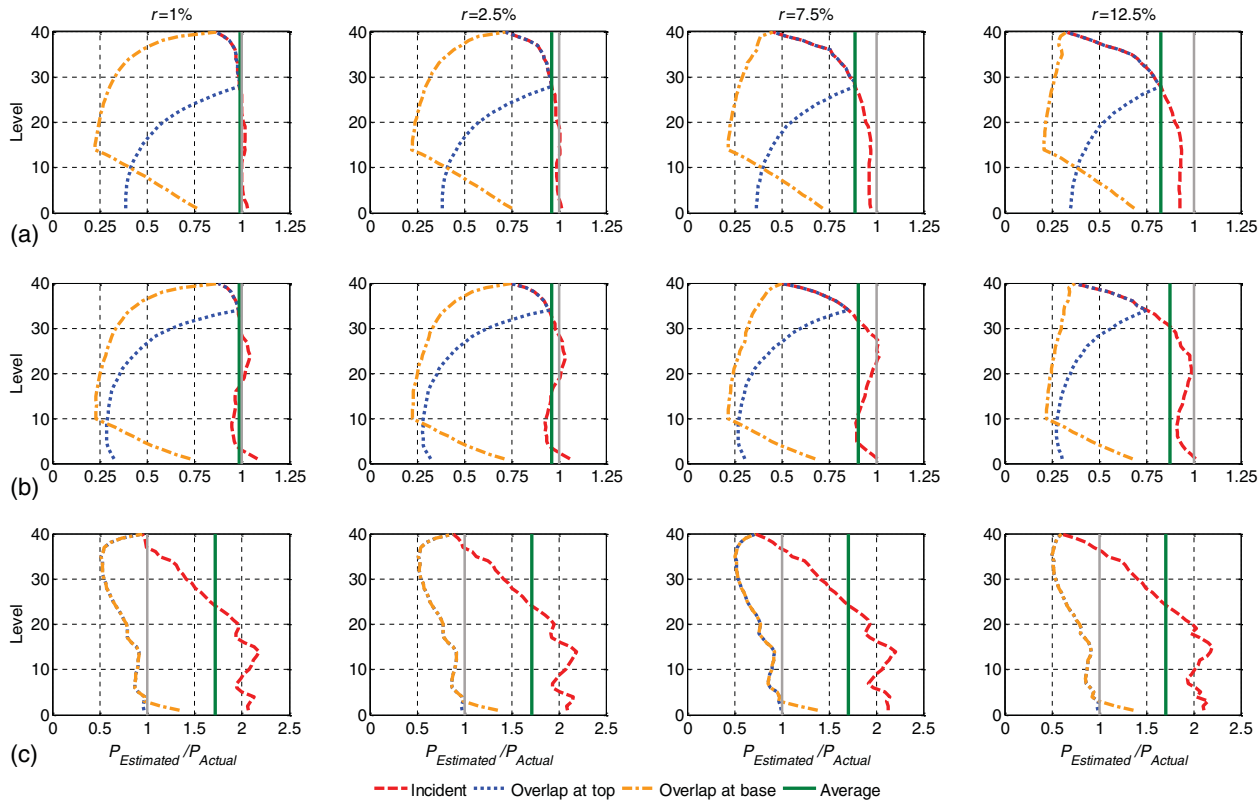

Fig. 12. Ratio of estimated to actual axial force demand in columns of shear-type BRB frames with different strain hardening ratios, subjected to (a) 1994 Northridge, Newhall-W.Pico Canyon Rd.; (b) 1999 Kocaili, Yarimca; and (c) 1952 Kern County, LA Hollywood Stor FF earthquake records with condensed time scale.

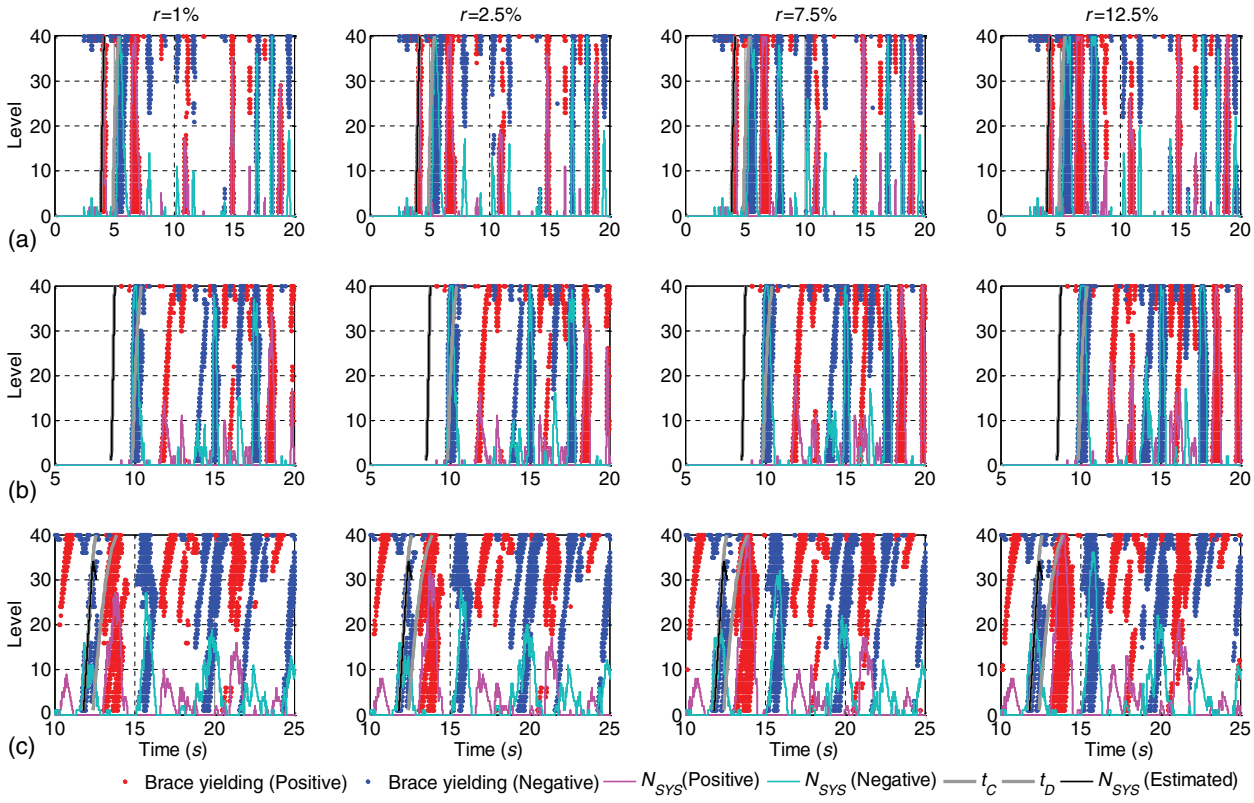

Fig. 13. Actual and estimated time history of brace yielding and number of simultaneously yielding stories (N_{SYS}) of shear-type BRB frames with different strain hardening ratios, subjected to (a) 1994 Northridge, Newhall-W.Pico Canyon Rd.; (b) 1999 Kocaili, Yarimca; and (c) 1952 Kern County, LA Hollywood Stor FF earthquake records with original time scale.

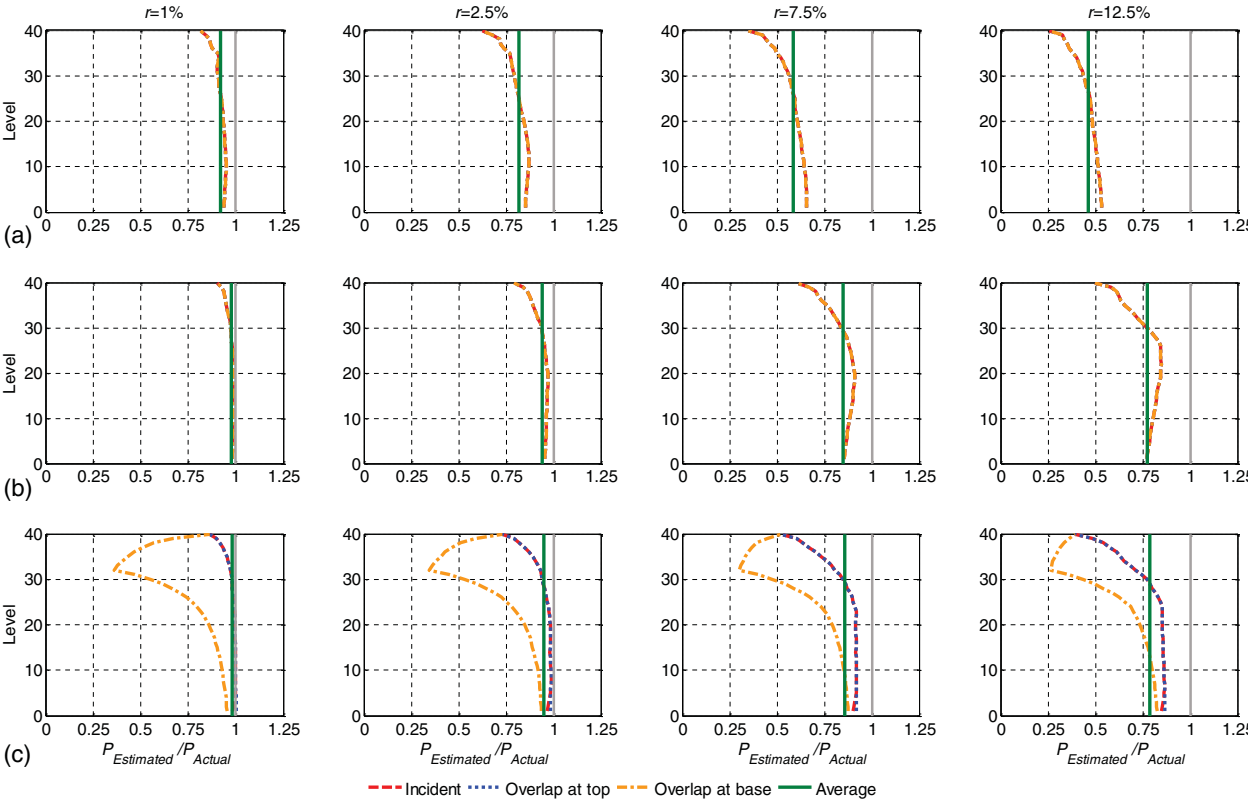

Fig. 14. Ratio of estimated to actual axial force demand in columns of shear-type BRB frames with different strain hardening ratios, subjected to (a) 1994 Northridge, Newhall-W.Pico Canyon Rd.; (b) 1999 Kocaili, Yarimca; and (c) 1952 Kern County, LA Hollywood Stor FF earthquake records with original time scale.

Strain Hardening over the Building Height

Condensed Time Scale

To check the extent of strain hardening attained by the braces over the height of the building, the ratio of the axial force of a brace P to its yield capacity P_y over the height of the building at different times is shown in Fig. 15 for a shear-type BRB frame with $r = 5\%$ (which corresponds approximately to the average value of strain hardening ratios in BRBs) subjected to the three earthquakes considered, with condensed time scale. For the first two earthquakes, the instants considered are when stories 1, 5, 10, 15, 20, 25, 30, and 35 reached their maximum strain-hardened strength as the incident wave traveled up the building. For the third earthquake, since not all the stories yielded, the P:P_y values are shown at arbitrarily chosen time intervals, starting at the time when the main pulse enters the building. The ratio of the maximum absolute axial force of the brace $|P|_{\max}$ to its corresponding yield capacity P_y is also shown in the figure.

As the incident wave travels up the building, when a particular story reaches its maximum strain-hardened strength, other stories that yield have P:P_y values greater than 1, but they do not touch the $|P|_{\max}$:P_y curve. For example, for the 1994 Northridge, Newhall-W. Pico Canyon Rd. (WPI046) earthquake, when the brace axial force at story 15 reaches its maximum value at 1.84 s, stories 15–34 yield simultaneously, as can be seen from the closer view of the story yielding pattern shown in Fig. 16 (which also shows the story yield patterns for the other two earthquakes). Accordingly, those stories have P:P_y values greater than 1. However, the results touch the $|P|_{\max}$:P_y curve only at story 15. While story yielding occurs once the value of the Δu:t_h wave exceeds the v_y value at that story, maximum strain-hardened strength occurs at peak displacement (i.e., peak ductility) due to the peak of the wave. Note that Δu:t_h is the ratio of the interstory drift Δu to the time t_h taken by the wave to travel through a story with height h. The value of Δu:t_h at a story will be equal to the value of the summation of the negative of the forward moving velocity wave and the backward moving velocity wave (i.e., $-v_f + v_b$). A curve joining the Δu:t_h value at all stories of the building at a given time will be referred to as the Δu:t_h wave (Shrestha and Bruneau 2016, 2017b). Thus, as the peak of the Δu:t_h wave propagates up the building height, the maximum strain-hardened strength at the stories occurs. The axial force time history shown in Fig. 17(a), together with a closer view of the forces around the time that the incident wave moves up the building shown in Fig. 17(b), indicate that the stories attain their maximum strength values serially as the wave propagate along the building height. This is an important observation, because some design specifications currently require that the maximum probable strength at each story over the height of the structure (i.e., the fully strain-hardened value) be used in performing capacity design of columns. The figure shows the axial force time history of the braces at different stories.

Similar observations can be made from the P:P_y profile for the second earthquake record. For the third earthquake record, which is a nonpulse-type earthquake, the story yielding due to the main pulse could not be predicted as systematically as for the first two earthquakes because of the interference from the preceding pulses in the velocity record (see Fig. 16). The P:P_y values are more than one and are close to the $|P|_{\max}$:P_y curve at few stories (Fig. 15).

Fig. 18 shows the variation of force reduction factor R, ductility μ, and $|P|_{\max}$:P_y over the height of the BRB frame with $r = 1$, 5, and 10% subjected to the three earthquakes with condensed time scale. The shape of the R, μ, and $|P|_{\max}$:P_y profiles

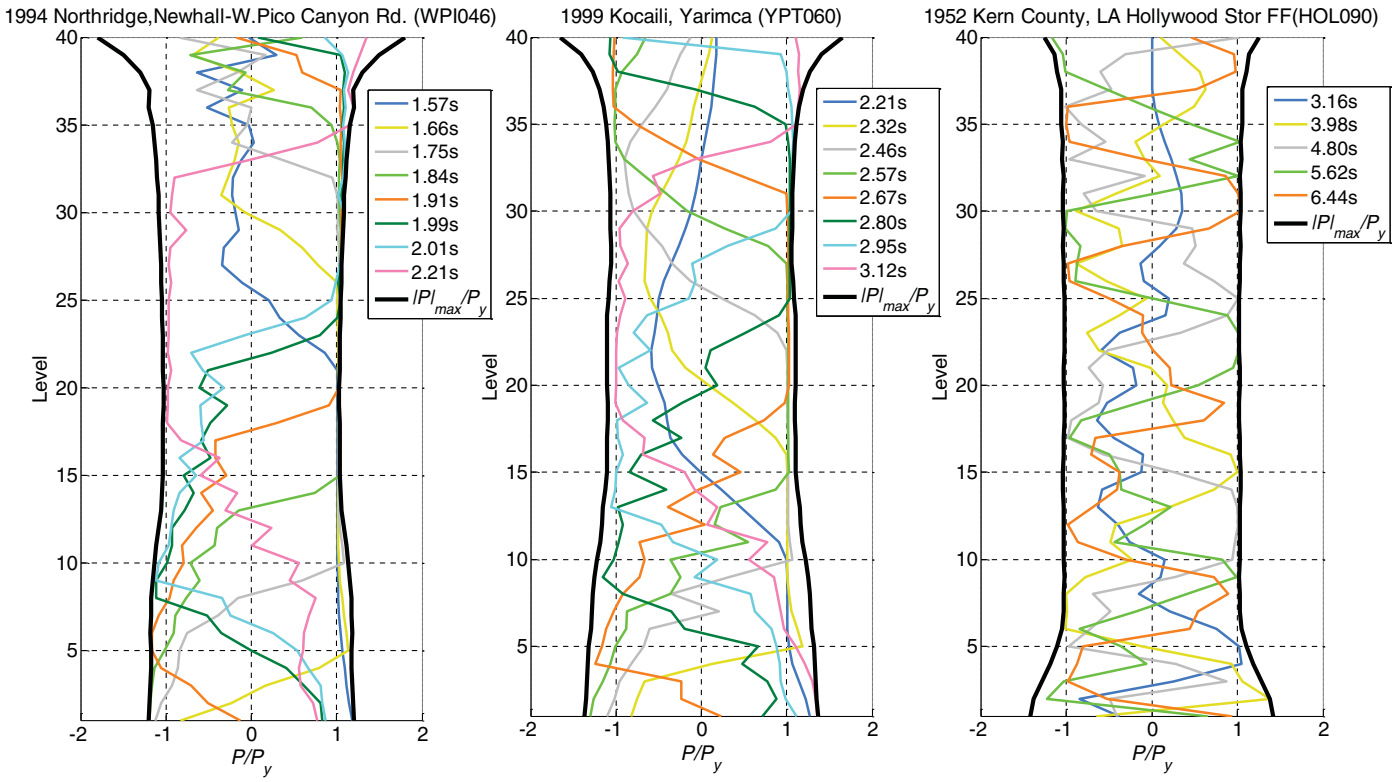

Fig. 15. Strain hardened axial force at the brace, normalized by its yield strength, at different times over the height of a shear-type BRB frame with $r = 5\%$ subjected to earthquakes with condensed time scale.

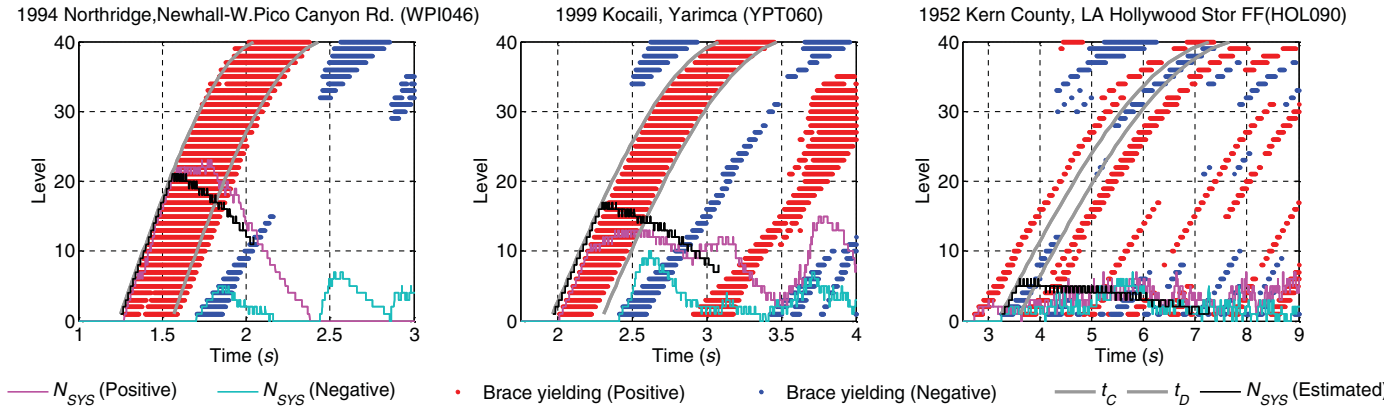

Fig. 16. Actual and estimated time history of brace yielding and number of simultaneously yielding stories (N_{SYS}) of a shear-type BRB frame with $r = 5\%$ subjected to earthquakes with condensed time scale.

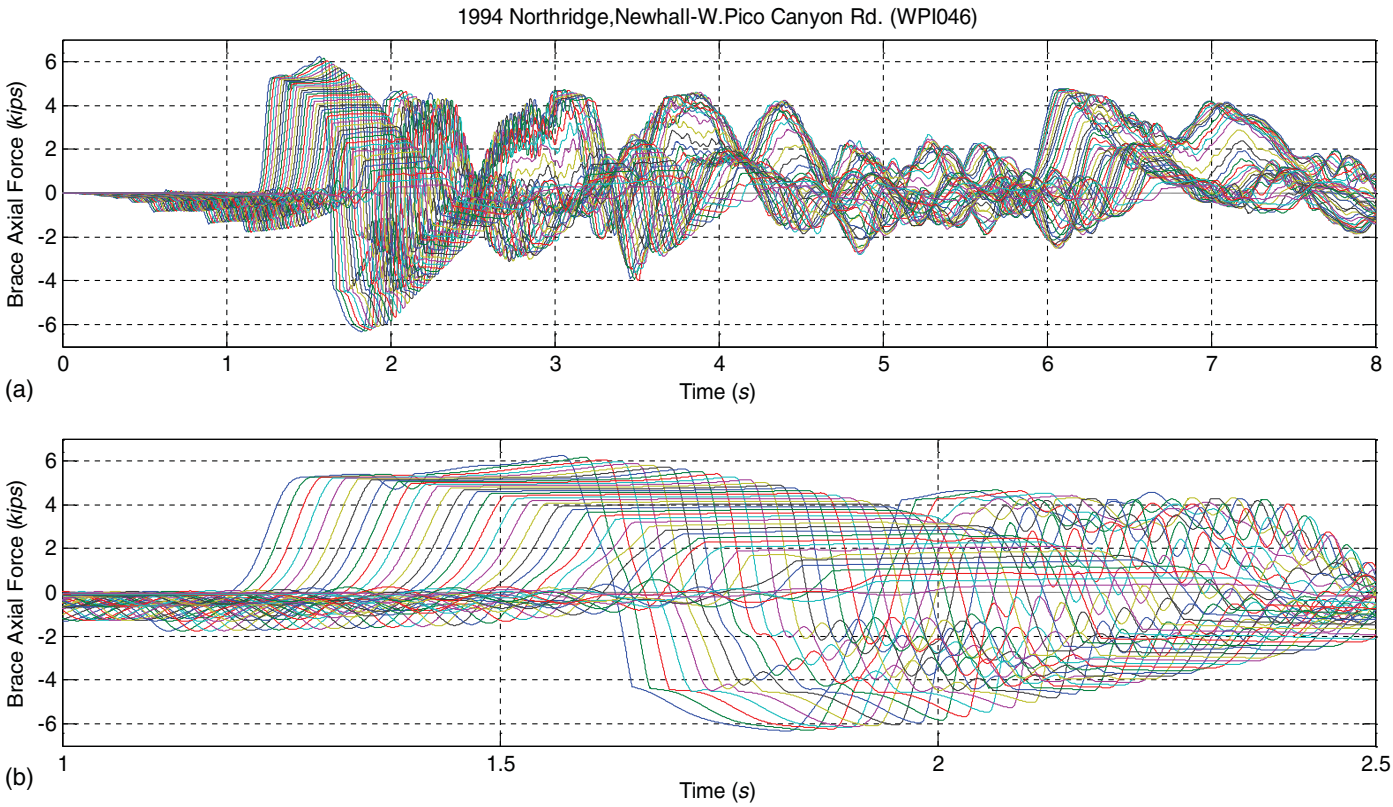

Fig. 17. (a) Axial force time history of the braces at different stories for shear-type BRB frames with $r = 5\%$ subjected to 1994 Northridge, Newhall-W.Pico Canyon Rd. (WPI046) record with condensed time scale; and (b) magnified view of axial force time history.

were found to be similar. In an ideal case, if the value of R and μ were constant over the height of the building, the resulting $|P|_{\max}$:P_y would also be same over the stories. When a particular story reached its maximum P:P_y value, the topmost story within the band of simultaneously yielding stories would just be starting to yield. If P:P_y was (conservatively) assumed to be linear between these two stories, the average $|P|_{\max}$:P_y over the simultaneously yielding stories would be equal to half of the maximum strain hardening value. On the basis of this ideal scenario and observations made for the BRB frame and the earthquakes considered in the study, when determining the maximum axial force to consider in the design of columns, the consideration that the maximum strain-hardened strength has been developed in all the stories above the particular story whose axial force demand is being estimated could be overconservative.

Original Time Scale

When earthquakes with original time scale are considered, due to the long duration of the main pulse of the earthquakes, the maximum axial force in the braces is not necessarily due to the incident wave; it could be due to the constructive overlaps of the velocity waves, as seen in the axial force time history shown in Fig. 19 for

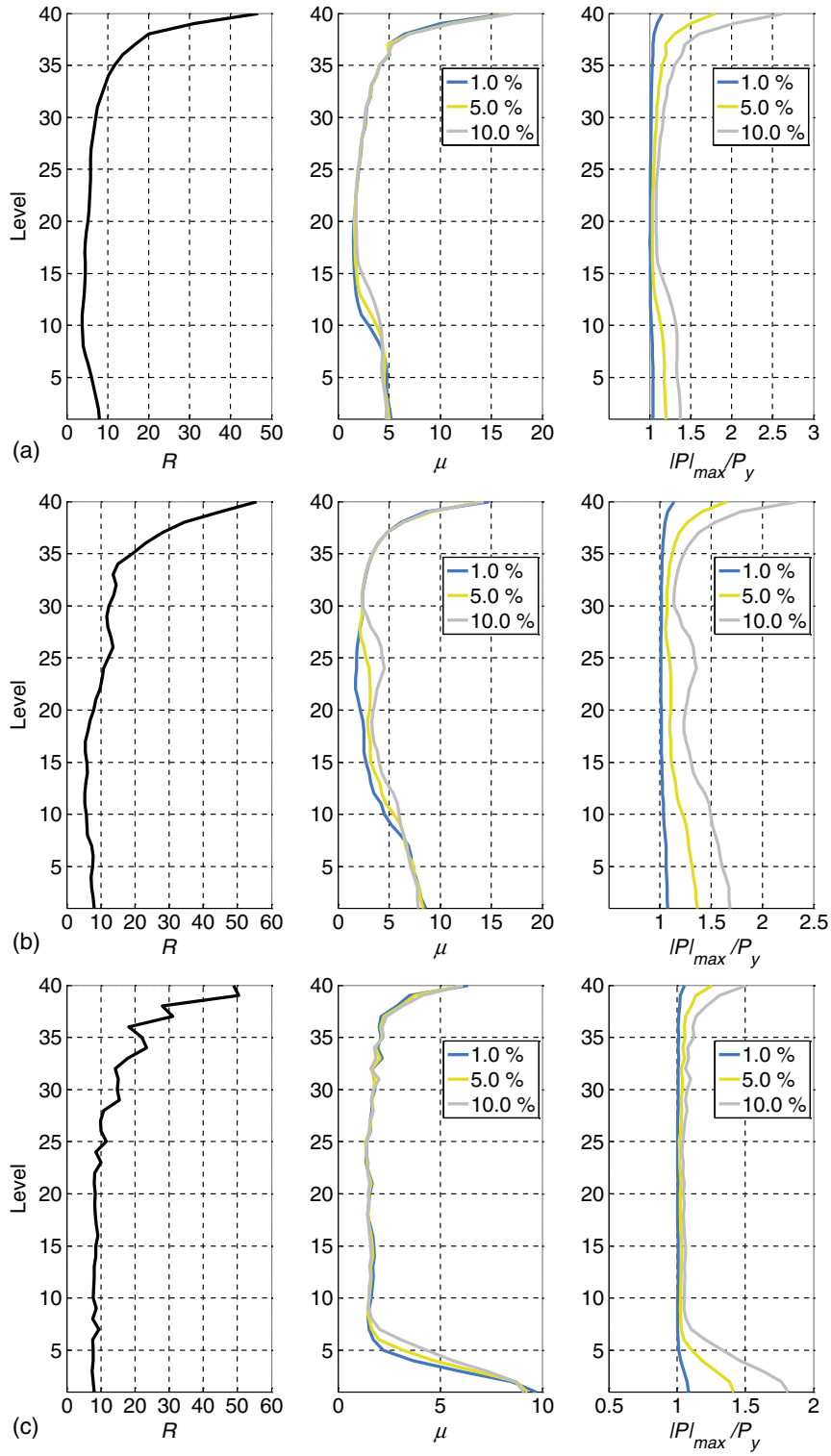

Fig. 18. Variation of force reduction factor R, ductility μ, and maximum absolute strain hardened axial force of the brace $|P|_{\max}$ normalized by its yield strength P_y over the height of a shear-type BRB frame with $r = 1$, 5, and 10% subjected to (a) 1994 Northridge, Newhall-W.Pico Canyon Rd. (WPI046); (b) 1999 Kocaili, Yarimca (YPT060); and (c) 1952 Kern County, LA Hollywood Stor FF (HOL090) earthquake records with condensed time scale.

the BRB frame with $r = 5\%$ subjected to the 1994 Northridge Earthquake record (WPI046). The beginning, peak, and end of the first half of the main pulse of the record entered the building at 3.72, 4.86, and 5.18 s, respectively, and reached the top of the building at 4.14, 5.28, and 5.6 s, respectively. However, the axial force at the stories reached peak values after 5.55 s.

Fig. 20 shows the P:P_y values at different stories of a shear-type BRB frame with $r = 5\%$ subjected to the three earthquakes with original time scale. The figure shows P:P_y profiles at different instants, after the brace in the first story reached maximum axial force. For the three earthquakes considered, P:P_y is more than 1 and close to $|P|_{\max}$:P_y at almost all the stories for at least three

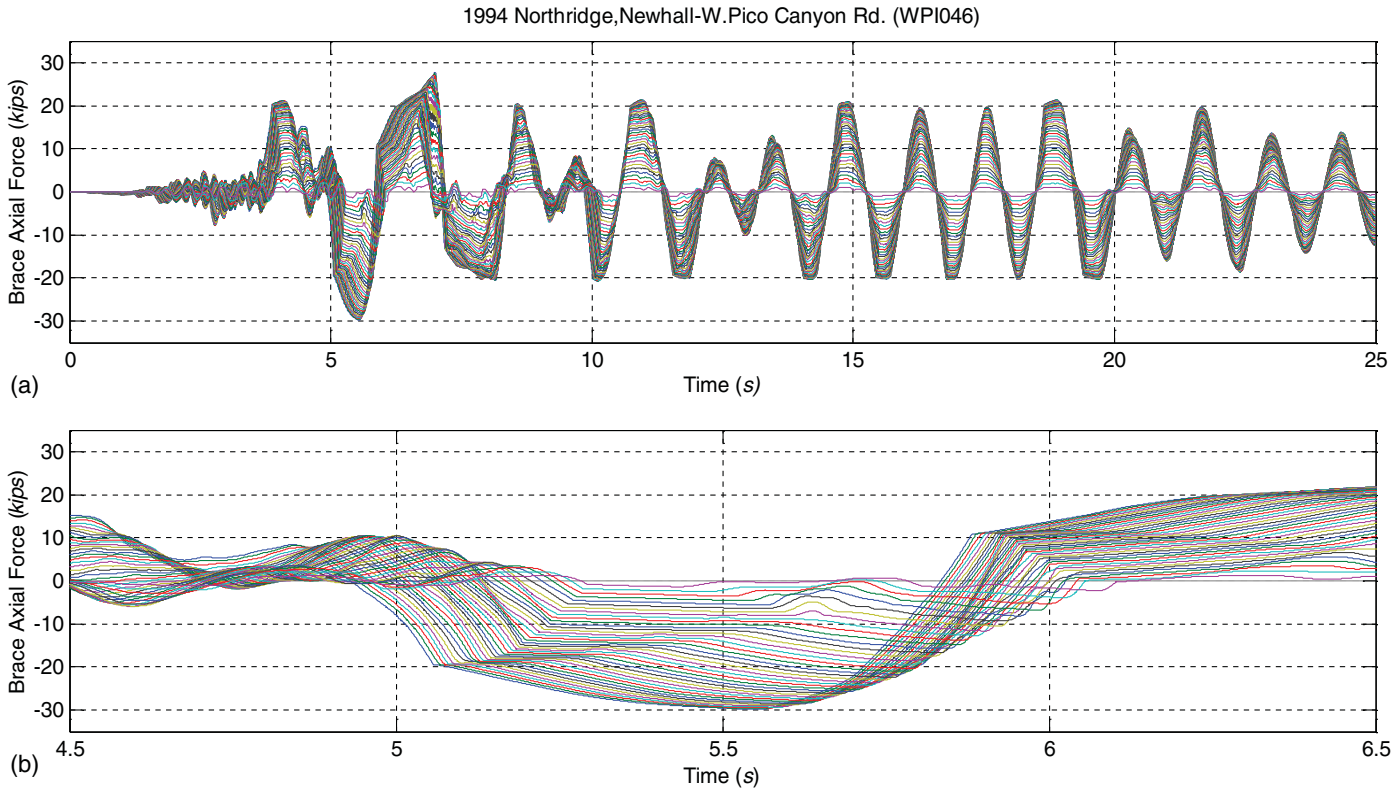

Fig. 19. (a) Axial force time history of the braces at different stories of a shear-type BRB frame with $r = 5\%$ subjected to earthquakes with original time scale; and (b) magnified view of axial force time history.

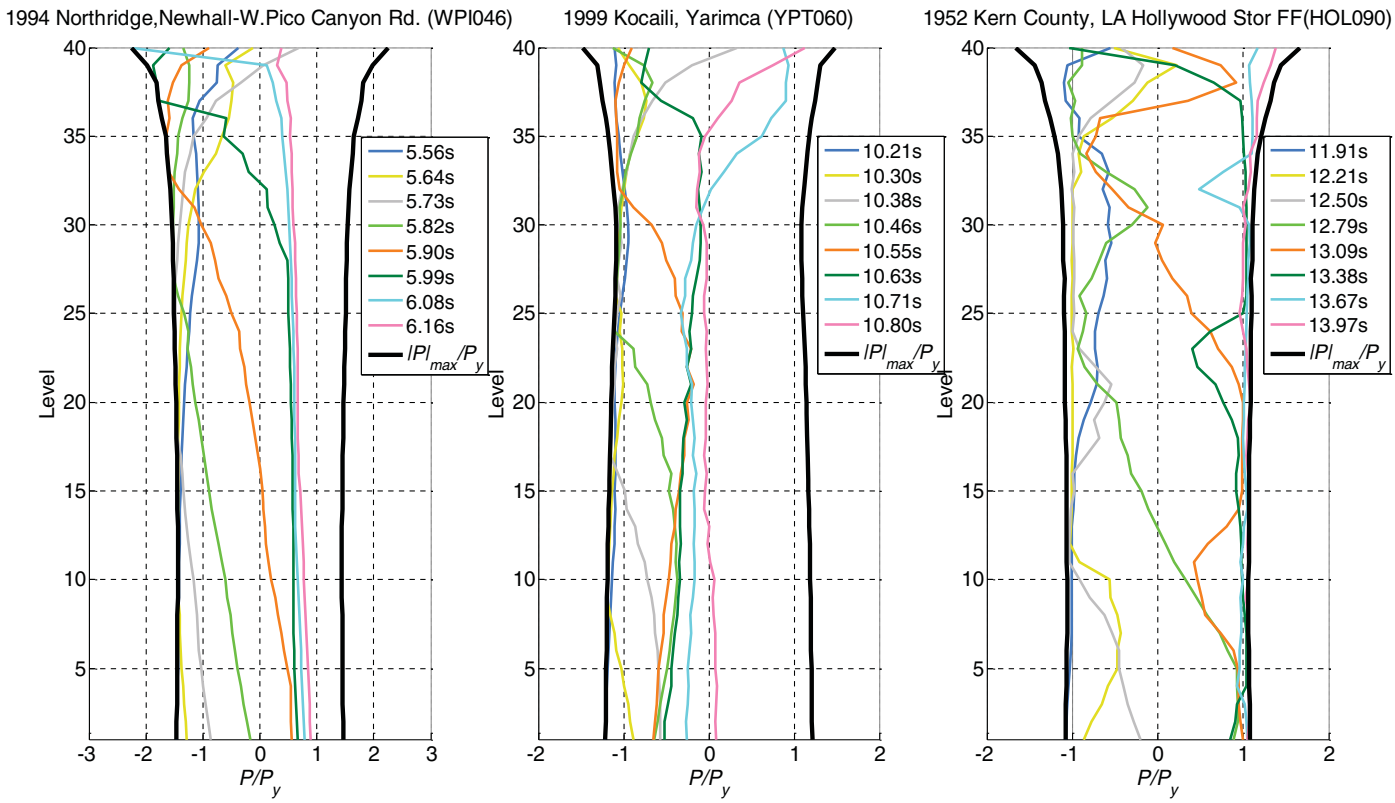

Fig. 20. Strain hardened axial force at the brace P normalized by its yield strength P_y at different times, over the height of a shear-type BRB frame with $r = 5\%$ subjected to earthquakes with original time scale.

of the specific times plotted. Therefore, in cases of earthquake records with large pulse duration ($0.5t_d$:$t_H > 1$), the conservative approach of considering the maximum value of strain-hardened strength over all of the stories undergoing simultaneous yielding may be more appropriate.

Conclusion

A previously developed method to estimate the number of simultaneously yielding stories in a shear-type building subjected to an earthquake excitation was used to formulate a procedure for estimating the axial force demands in columns of such frames. In this procedure, axial force demand is estimated by summing the vertical force transferred by the N_{SYS} simultaneously yielding stories with the SRSS of the rest of the vertical component of the braces' yield strengths above the story under consideration. A parametric study was also conducted to verify the adequacy of the procedure and the sensitivity of the results for different values of column-to-brace stiffness ratio k_{col}:k_{br} and strain hardening ratio r. The main observations and findings of the study are as follows:

1. The procedure for estimating the axial force demand in columns gave values close to the actual values for most of the stories, especially for earthquakes with more noticeable velocity pulses. Since the estimation procedure does not consider strain hardening, it slightly underestimated the axial force demands for original earthquakes (not condensed time scale) and at the upper stories for earthquakes with condensed time scale.
2. A parametric study considering values of column-to-brace stiffness ratio ranging from 0.01 to 1.0 and strain hardening ratio ranging from 1.0 to 12.5% showed that the estimation procedure still worked effectively for these cases. With increases in the column-to-brace stiffness ratio, the N_{SYS} value was found to increase; this effect was prominent in case of earthquakes with condensed time scale. Also, with increases in strain hardening, there was an increase in the discrepancy between the estimated and the actual axial force demand.
3. The simultaneously yielding stories do not reach their maximum strain-hardened strength at the same time. For the frames and the earthquakes considered in this study, the consideration that the maximum strain-hardened strength has been developed at all the stories above the story whose axial force demand is being estimated would yield overconservative values for earthquakes with short duration main pulse. However, for earthquakes with long-duration main pulse, the strain-hardened strengths over the height of the frames analyzed were close to the maximum values at many stories; therefore, in such cases, consideration of maximum strain-hardened strength over all the stories above the story whose axial force demand was being estimated would be appropriate.

Acknowledgments

This research was partly supported by the MCEER at the University at Buffalo. Any opinions, findings, conclusions, or recommendations in this paper, however, are solely those of the authors and do not necessarily reflect the views of the sponsors.

References

AISC. 2010. *Seismic provisions for structural steel buildings*. ANSI/AISC 341-10. Chicago: AISC.

Baker, J. W. 2007. "Quantitative classification of near-fault ground motions using wavelet analysis." *Bull. Seismol. Soc. Am.* 97 (5): 1486–1501. https://doi.org/10.1785/0120060255.

Bruneau, M., C. Uang, and R. Sabelli. 2011. *Ductile design of steel structures*. New York: McGraw-Hill.

Bruneau, M., and N. Wang. 1996a. "Normalized energy-based methods to predict the seismic ductile response of SDOF structures." *Eng. Struct. J.* 18 (1): 13–28. https://doi.org/10.1016/0141-0296(95)00100-3.

Bruneau, M., and N. Wang. 1996b. "Some aspects of energy methods for the inelastic seismic response of ductile SDOF structures." *Eng. Struct. J.* 18 (1): 1–12. https://doi.org/10.1016/0141-0296(95)00099-X.

Clough, R. W., and J. Penzien. 2003. *Dynamics of structures*. Walnut Creek, CA: Computers & Structures.

Dicleli, M., and M. Bruneau. 1995. "An energy approach to sliding of simple-span simply supported slab-on-girder steel highway bridges with damaged bearings." *J. Earthquake Eng. Struct. Dyn.* 24 (3): 395–409. https://doi.org/10.1002/eqe.4290240307.

Ebrahimian, M., and M. I. Todorovska. 2014. "Wave propagation in a timoshenko beam building model." *J. Eng. Mech.* 140 (5): 04014018. https://doi.org/10.1061/(ASCE)EM.1943-7889.0000720.

Hall, J. F., T. H. Heaton, M. W. Halling, and D. J. Wald. 1995. "Near-source ground motion and its effects on flexible buildings." *Earthquake Spectra* 11 (4): 569–605. https://doi.org/10.1193/1.1585828.

Humar, J. L. 2002. *Dynamics of structures*. Tokyo, Japan: A.A. Balkema.

Kalkan, E., and S. K. Kunnath. 2006. "Effects of fling step and forward directivity on seismic response of buildings." *Earthquake Spectra* 22 (2): 367–390. https://doi.org/10.1193/1.2192560.

Krishnan, S., and M. Muto. 2012. "Mechanism of collapse of tall steel moment-frame buildings under earthquake excitation." *J. Struct. Eng.* 138 (11): 1361–1387. https://doi.org/10.1061/(ASCE)ST.1943-541X.0000573.

Lacerte, M., and R. Tremblay. 2006. "Making use of brace overstrength to improve the seismic response of multistory split-X concentrically braced steel frames." *Can. J. Civ. Eng.* 33 (8): 1005–1021. https://doi.org/10.1139/l06-035.

Mavroeidis, G. P., and A. S. Papageorgiou. 2003. "A mathematical representation of near-fault ground motions." *Bull. Seismol. Soc. Am.* 93 (3): 1099–1131. https://doi.org/10.1785/0120020100.

Redwood, R. G., and V. S. Channagiri. 1991. "Earthquake resistant design of concentrically braced frame." *Can. J. Civ. Eng.* 18 (5): 839–850. https://doi.org/10.1139/l91-101.

Richards, P. W. 2009. "Seismic column demands in ductile braced frames." *J. Struct. Eng.* 135 (1): 33–41. https://doi.org/10.1061/(ASCE)0733-9445(2009)135:1(33).

Şafak, E. 1999. "Wave propagation formulation of seismic response of multi-story buildings." *J. Struct. Eng.* 125 (4): 426–437. https://doi.org/10.1061/(ASCE)0733-9445(1999)125:4(426).

Shrestha, L., and M. Bruneau. 2016. *Seismic demand in columns of steel frames*. Technical Rep. MCEER-16-0002. Buffalo, NY: Univ. at Buffalo.

Shrestha, L., and M. Bruneau. 2017a. "Estimating number of simultaneously yielding stories in a shear building subjected to earthquake excitation." *Eng. Struct.* 148: 552–570.

Shrestha, L., and M. Bruneau. 2017b. "Estimating number of simultaneously yielding stories in a shear building subjected to full-sine pulse velocity base excitation." *Eng. Struct.* 134: 236–252. https://doi.org/10.1016/j.engstruct.2016.12.023.

Snieder, R., and E. Şafak. 2006. "Extracting the building response using seismic interferometry: Theory and application to the Millikan library in Pasadena, California." *Bull. Seismol. Soc. Am.* 96 (2): 586–598. https://doi.org/10.1785/0120050109.

Todorovska, M. I., and M. T. Rahmani. 2013. "System identification of buildings by wave travel time analysis and layered shear beam models: Spatial resolution and accuracy." *Struct. Control Health Monit.* 20 (5): 686–702. https://doi.org/10.1002/stc.1484.

Todorovska, M. I., and M. D. Trifunac. 2008a. "Earthquake damage detection in the Imperial County Services Building III: Analysis

of wave travel times via impulse response functions." *Soil Dyn. Earthquake Eng.* 28 (5): 387–404. https://doi.org/10.1016/j.soildyn.2007.07.001.

Todorovska, M. I., and M. D. Trifunac. 2008b. "Impulse response analysis of the Van Nuys 7-storey hotel during 11 earthquakes and earthquake damage detection." *Struct. Control Health Monit.* 15 (1): 90–116. https://doi.org/10.1002/stc.208.

Tremblay, R., and N. Robert. 2001. "Seismic performance of low- and medium-rise chevron braced frames." *Can. J. Civ. Eng.* 28 (4): 699–714. https://doi.org/10.1139/l01-038.

Vissiliou, M. F., and N. Makris. 2011. "Estimating time scales and length scales in pulselike earthquake acceleration records with wavelet analysis." *Bull. Seismol. Soc. Am.* 101 (2): 596–618. https://doi.org/10.1785/0120090387.